THE JOURNAL OF BIOLOGICAL CHEMISTRY VOL. 290, NO. 43, pp. 26072–26087, October 23, 2015

Glyceraldehyde-3-phosphate Dehydrogenase Aggregates Accelerate Amyloid-β Amyloidogenesis in Alzheimer Disease*

Received for publication, June 2, 2015, and in revised form, August 31, 2015 Published, JBC Papers in Press, September 10, 2015, DOI 10.1074/jbc.M115.669291

Masanori Itakura[‡1], Hidemitsu Nakajima[‡1,2], Takeya Kubo[‡], Yuko Semi[‡], Satoshi Kume[§], Shusaku Higashida[‡], Akihiro Kaneshige[‡], Mitsuru Kuwamura[¶], Naoki Harada[‖], Akinori Kita[‡], Yasu-Taka Azuma[‡], Ryoichi Yamaji[‖], Takashi Inui[§], and Tadayoshi Takeuchi[‡]

From the [‡]Laboratory of Veterinary Pharmacology, Graduate School of Life and Environmental Sciences, and [¶]Laboratory of Veterinary Pathology, Osaka Prefecture University, Osaka 5988531 and the Laboratories of [§]Biological Macromolecules and [‖]Nutrition Chemistry, Osaka Prefecture University, Osaka 5998531, Japan

Background: There is currently no strong evidence for a linkage between glyceraldehyde-3-phosphate dehydrogenase (GAPDH) and Alzheimer disease (AD).
Results: GAPDH aggregates enhanced amyloid-β peptide (Aβ) amyloidogenesis and augmented Aβ40-induced neurotoxicity, both *in vitro* and *in vivo*, concomitant with mitochondrial dysfunction.
Conclusion: GAPDH aggregates accelerate Aβ amyloidogenesis.
Significance: Aβ amyloidogenesis associated with GAPDH aggregation might underlie AD pathogenesis.

Alzheimer disease (AD) is a progressive neurodegenerative disorder characterized by loss of neurons and formation of pathological extracellular deposits induced by amyloid-β peptide (Aβ). Numerous studies have established Aβ amyloidogenesis as a hallmark of AD pathogenesis, particularly with respect to mitochondrial dysfunction. We have previously shown that glycolytic glyceraldehyde-3-phosphate dehydrogenase (GAPDH) forms amyloid-like aggregates upon exposure to oxidative stress and that these aggregates contribute to neuronal cell death. Here, we report that GAPDH aggregates accelerate Aβ amyloidogenesis and subsequent neuronal cell death both *in vitro* and *in vivo*. Co-incubation of Aβ40 with small amounts of GAPDH aggregates significantly enhanced Aβ40 amyloidogenesis, as assessed by *in vitro* thioflavin-T assays. Similarly, structural analyses using Congo red staining, circular dichroism, and atomic force microscopy revealed that GAPDH aggregates induced Aβ40 amyloidogenesis. In PC12 cells, GAPDH aggregates augmented Aβ40-induced cell death, concomitant with disruption of mitochondrial membrane potential. Furthermore, mice injected intracerebroventricularly with Aβ40 co-incubated with GAPDH aggregates exhibited Aβ40-induced pyramidal cell death and gliosis in the hippocampal CA3 region. These observations were accompanied by nuclear translocation of apoptosis-inducing factor and cytosolic release of cytochrome *c* from mitochondria. Finally, in the 3×Tg-AD mouse model of AD, GAPDH/Aβ co-aggregation and mitochondrial dysfunction were consistently detected in an age-dependent manner, and Aβ aggregate formation was attenuated by GAPDH siRNA treatment. Thus, this study suggests that GAPDH aggregates accelerate Aβ amyloidogenesis, subsequently leading to mitochondrial dysfunction and neuronal cell death in the pathogenesis of AD.

Glyceraldehyde-3-phosphate dehydrogenase (GAPDH) has been identified as a key enzyme in glycolysis. Several reports further reveal that GAPDH has a variety of other functions, including DNA repair (1), transcriptional regulation (2), membrane fusion and transport (3), autophagy (4), and cell death (5–8). Upon exposure to oxidative stress, GAPDH binds Siah (5) and undergoes nuclear translocation. Nuclear GAPDH then induces p53-dependent transcription of apoptotic genes (9). We have previously reported that GAPDH also forms oxidative stress-induced aggregates, which is followed by the production of amyloid-like fibrils, eventually resulting in cell death (7, 10). Similarly, in mice treated with methamphetamine, which causes widespread oxidative stress in the brain, there is evidence of GAPDH aggregation and neuronal cell death (11). Furthermore, GAPDH transgenic mice have enhanced neuronal cell death accompanied by robust aggregation of GAPDH (11).

Abnormal protein aggregation has been suggested as a possible underlying mechanism in the pathogenesis of several neurodegenerative disorders (12, 13), and an increasing number of studies implicate GAPDH aggregation in this process (14–17). Indeed, GAPDH aggregates have been found post mortem in the brains of patients with neurodegenerative disorders, particularly Alzheimer disease (AD).[3] However, details regarding its involvement in the development of AD remain unclear (18–23).

* This work was supported in part by Grants-in-aid for Scientific Research 22580339 and 25450428 (to H. N.) from the Japan Society for the Promotion of Science, by Grants-in-aid from the Japan Science and Technology Agency for exploratory research in A-STEP AS232Z02185G and AS242Z02311Q (to H. N.), he Adaptable and Seamless Technology Transfer Program through target-driven R&D, and by Grant-in-aid for Scientific Research on Innovative Areas 02120076 (to T. I.). The authors declare that they have no conflicts of interest with the contents of this article.
[1] Both authors contributed equally to this work.
[2] To whom correspondence should be addressed: Laboratory of Veterinary Pharmacology, Graduate School of Life and Environmental Sciences, Osaka Prefecture University, Izumisano 5988531, Osaka, Japan. Tel.: 81-72-463-5274; Fax: 81-72-463-5264; E-mail: hnakajima@vet.osakafu-u.ac.jp.

[3] The abbreviations used are: AD, Alzheimer disease; Aβ, amyloid-β peptide; AFM, atomic force microscopy; AIF, apoptosis-inducing factor; GFAP, glial fibrillary acidic protein; i.c.v., intracerebroventricular; ThT, thioflavin-T; 3xTg, triple transgenic mice.

AD is the most common cause of adult onset dementia, characterized by neuronal cell loss, senile plaques, and extensive gliosis in the cortex and hippocampus (24). There is good evidence suggesting that aggregation of amyloid-β peptide (Aβ), a major component of senile plaques, occurs both intracellularly and extracellularly and that this aggregation is a primary event in the pathogenesis of AD (25–27). During aggregation, Aβ preferentially adopts the less soluble β-sheet structure, rather than the more soluble random coil and α-helix structures, leading to formation of oligomers and fibrils (28).

Mitochondrial dysfunction is a hallmark of Aβ-induced neurotoxicity in AD (29). Extracellular Aβ aggregates bind to the plasma membrane, stimulating aberrant Ca^{2+} influx, which then leads to disruption of mitochondrial membrane potential (30). Intracellular Aβ aggregates have recently been associated with the disruption of mitochondrial membrane potential via interaction with various mitochondrial proteins (31). Aβ aggregates cause massive increases in mitochondrial membrane permeability and stimulate the release of small pro-apoptotic proteins, including apoptosis-inducing factor (AIF) and cytochrome *c* (32).

To date, several lines of evidence point to an association between GAPDH and AD (18, 20, 33, 34). In post-mortem brain samples from AD patients, GAPDH has been found in senile plaques, and disulfide-bonded GAPDH aggregates have been found in the detergent-insoluble fraction (17, 18). Other than what has been revealed by these studies, little is known about the significance of GAPDH aggregation in the context of AD pathogenesis.

Based on these findings, we hypothesize that GAPDH aggregation might be involved in Aβ amyloidogenesis, thereby contributing to AD pathogenesis. In this study, we first show enhancement of Aβ40 amyloidogenesis when co-incubated with GAPDH aggregates *in vitro*. We then demonstrate that GAPDH aggregates potentiate Aβ40-induced neurotoxicity, accompanied by mitochondrial dysfunction *in vitro* and *in vivo*. The triple transgenic mouse model of AD (3×Tg-AD), which exhibits both intracellular and extracellular age-dependent Aβ aggregation (25), is often used in studies investigating AD pathogenesis (35). Therefore, we also examined the link between GAPDH aggregation and AD pathogenesis in 3×Tg-AD mice. Our results suggest that there is an interaction between GAPDH and Aβ aggregates in the cortical extracellular deposits (the so-called human senile plaques) and hippocampal CA3 pyramidal neurons of these mice.

Experimental Procedures

Chemicals and Antibodies—Unless otherwise noted, chemicals were of analytical grade. Aβ40 (HCl salt), Aβ42 (trifluoroacetate form), and Aβ(25–35) (trifluoroacetate form) were purchased from the Peptide Institute (Osaka, Japan). Thioflavin-T (ThT), Congo red, and rhodamine 123 were purchased from Sigma (Tokyo, Japan). The NO generator, (±)-(*E*)-4-ethyl-2-[(*E*)-hydroxyimino]-5-nitro-3-hexenamide, and DAPI were purchased from DOJINDO (Kumamoto, Japan). Primary antibodies, including mouse anti-Aβ monoclonal antibody (6E10, Covance, Princeton, NJ), rabbit anti-AIF polyclonal antibody (R&D Systems, Minneapolis, MN), rabbit anti-H2B polyclonal antibody (Upstate Biotechnology, Lake Placid, NY), mouse anti-cytochrome *c* monoclonal antibody (BD Biosciences), and mouse anti-glial fibrillary acidic protein (GFAP) monoclonal antibody (DAKO Japan, Kyoto, Japan), were purchased from the indicated companies. Rabbit anti-GAPDH polyclonal antibody was prepared in-house (36). Secondary antibodies, including goat anti-rabbit IgG and goat anti-mouse IgG, were purchased from Invitrogen. Control siRNA (5′-UGGUUUACAUGUCGACUAA-3′) and Accell mouse GAPDH siRNA (5′-UCGUGGAGUCUACUGGUGU-3′) were purchased from Dharmacon-Thermo Fisher Scientific (Lafayette, CO).

Preparation of Aβ40 Solution—A lyophilized powder of Aβ40 was dissolved in a solution of 0.02% ammonia at a stock concentration of 1 mM by brief stirring. Aliquots were stored at −80 °C prior to use. The reaction solution of Aβ40 was diluted with ice-cold PBS at a concentration of 50 μM at 4 °C and used immediately.

Cloning, Expression, and Purification of Human Recombinant GAPDH—Human *GAPDH* cDNA was generated, as described previously (7). For bacterial expression, cDNA was cloned into pBAD-HisA (Invitrogen) using the SacI-KpnI sites. The sequence of cloned human *GAPDH* cDNA was identical to that reported in GenBank™ (GenBank™ accession number M33197). The pBAD-HisA vector carrying human *GAPDH* cDNA was transformed into the *gap*(−) *Escherichia coli* strain, W3CG (37). Recombinant GAPDH protein was expressed and purified, as described previously (7). Briefly, the transformants were cultured for 2 h at 37 °C in M63 minimal medium containing 50 μg/ml ampicillin, 15 μg/ml tetracycline, and 0.2% (w/v) L-(+)-arabinose. After 24 h, cells expressing recombinant protein were collected by centrifugation (3000 × *g* for 15 min at 4 °C) and resuspended in a lysis buffer containing 50 mM sodium phosphate (pH 8.0), 300 mM NaCl, 30 mM imidazole, 10% glycerol, and 2 mM 2-mercaptoethanol. The suspensions were sonicated on ice and centrifuged at 15,000 × *g* for 30 min at 4 °C. The supernatants were incubated with nickel-nitrilotriacetic acid-agarose resin (50% slurry, Qiagen Japan, Tokyo, Japan) for 2 h at room temperature with shaking. Reduced proteins were loaded directly onto a PD-10 column (GE Healthcare UK Ltd.) equilibrated with G2 buffer containing 50 mM Tris-HCl (pH 8.0), 150 mM NaCl, 1 mM EDTA, and 5% glycerol. Protein concentrations were determined using spectrophotometry at 280 nm ($\epsilon_{0.1\%} = 1.0$).

Preparation of GAPDH Aggregates—The solution of GAPDH (0.6 mg/ml) was incubated, with 100 μM (±)-(*E*)-4-ethyl-2-[(*E*)-hydroxyimino]-5-nitro-3-hexenamide for 72 h at 37 °C, resulting in robust GAPDH aggregation (11). The incubated solution was centrifuged at 20,400 × *g* for 30 min at 25 °C, and the pellets were sonicated on ice in a buffer containing 20 mM Tris-HCl (pH 7.4), 100 mM NaCl, and 1 mM $MgCl_2$ for 10 min. The buffer was added at a concentration of 333 μM.

Amyloidogenesis, ThT Fluorescence Assay—To measure amyloidogenesis of Aβ40, Aβ42, and Aβ(25–35), ThT fluorescence assays were performed according to a previous report (38) with minor modifications. Briefly, a 10-μl sample was mixed with a 2-ml ThT solution (10 μM in 50 mM glycine-NaOH, pH 8.0), and fluorescence intensity was measured at wavelengths of 450 nm (excitation) and 482 nm (emission) using an RF-1500 fluo-

rescence spectrophotometer (Shimadzu, Kyoto, Japan). In the time course studies, the 50 μM Aβ40 solution was incubated for 6 days at 37 °C with or without the equivalent of 5 μM monomeric GAPDH aggregates (10% molar ratio to Aβ40), and fluorescence of the aliquot was measured every 24 h. In studies examining concentration dependence, the solution of Aβ40 at 50 μM was incubated with or without GAPDH aggregates (0.05, 0.5, and 5 μM; 0.1, 1, and 10%, respectively) at 37 °C, and fluorescence was measured on day 2. Alternatively, Aβ40 was incubated with 10% native (non-aggregated) GAPDH, and fluorescence was measured at day 2. The fluorescence intensities of Aβ42 (25 μM) and Aβ(25–35) (50 μM) were measured 1 h after incubation at 37 °C by the same method.

Congo Red Birefringence—The procedure for Congo red birefringence was carried out, as described previously (11), with minor modifications. Aliquots (40 μl) of Aβ40 at 50 μM with or without 10% GAPDH aggregates were incubated for 48 h (day 2) and added to a 360-μl Congo red solution (25 μg/ml in PBS). This mixture was incubated for 30 min at 25 °C and then centrifuged at 20,400 × *g* for 30 min at 4 °C. The resultant pellets were resuspended in 50 μl of sterilized Milli-Q water and then dried on a glass slide. Birefringence was observed with an Eclipse LV100POL microscope equipped with a polarizing stage (Nikon, Tokyo, Japan).

Circular Dichroism (CD)—The far-ultraviolet CD spectrum of Aβ40 at 50 μM treated with or without GAPDH aggregates at day 2 was measured at 37 °C with a spectropolarimeter (model J-820, Jasco, Tokyo, Japan). The path length of the optical quartz cuvette was 1.0 mm at 200–250 nm. Spectra were obtained as the average of eight successive scans with a bandwidth of 2.0 nm. These spectra are expressed as values subtracted from that of each vehicle. These data are expressed as molar residue ellipticity (θ).

Atomic Force Microscopy (AFM)—Aliquots (10 μl) of Aβ40 at 50 μM with or without GAPDH aggregates were incubated for 48 h (day 2), sonicated, and spotted onto freshly cleaved mica, incubated for 1 min, rinsed three times with water, and then dried. All measurements were carried out in "tapping mode" under ambient conditions using AFM (Nanoscope, Veeco Instruments Inc., Santa Barbara, CA) with single-beam silicon cantilever probes. We examined three regions of the mica surface to ensure that we obtained an accurate sample of structures on the mica (39).

Cell Viability—Cells from the rat pheochromocytoma cell line, PC12 (ATCC), were grown in Dulbecco's modified Eagle's medium/Ham's F-12 medium (DMEM/F-12, 1:1) supplemented with 10% fetal bovine serum, 2 mM glutamine, and antibiotics/antimycotics (Invitrogen) at 37 °C in a 5% CO_2 humidified incubator. Cell viability was measured using a Cell Titer Glo Luminescent Cell Viability Assay kit (Promega) according to the manufacturer's instructions (10, 11). PC12 cells ($3 \times 10^5/cm^2$) were seeded onto a 96-well plate coated with 0.1 mg/ml poly-D-lysine (Sigma) and grown for 24 h. In this study, PC12 cells were divided into six treatment groups as follows: 1) control, vehicle of DMEM/F-12, 1% fetal bovine serum; 2) aggregated Aβ40 (50 μM) incubated for 48 h at 37 °C in vehicle; 3) aggregated Aβ40 (50 μM) plus 0.1% GAPDH aggregates (0.05 μM) in vehicle; 4) aggregated Aβ40 (50 μM) plus 1% GAPDH aggregates (0.5 μM) in vehicle; 5) aggregated Aβ40 (50 μM) plus 10% GAPDH aggregates (5 μM) in vehicle; and 6) 10% GAPDH aggregates (5 μM) in vehicle. Treatment with these solutions was carried out for 72 h at 37 °C in a 5% CO_2 humidified incubator.

Mitochondrial Membrane Potential Assay—Mitochondrial membrane potential was measured using rhodamine 123 (40). PC12 cells ($3 \times 10^5/cm^2$) were seeded on glass coverslips coated with 0.1 mg/ml poly-D-lysine and grown for 24 h at 37 °C. In this study, PC12 cells were divided into four treatment groups as follows: 1) control, vehicle of DMEM/F-12, 1% fetal bovine serum; 2) aggregated Aβ40 (50 μM) incubated for 48 h at 37 °C in vehicle; 3) aggregated Aβ40 (50 μM) plus 10% GAPDH aggregates (5 μM) in vehicle; and 4) 10% GAPDH aggregates in vehicle. After treatment, the culture medium was replaced with DMEM/F-12 containing rhodamine 123 (5 μg/ml), followed by incubation for 10 min at 37 °C in a 5% CO_2-humidified incubator. After two washes with DMEM/F-12 and one wash with PBS, fluorescence from rhodamine 123-loaded cells was captured using a confocal scanning microscope (model C1si-TE2000-E, Nikon; excitation, 488 nm; emission, 525 nm). Raw images (500 × 500 μm) were first grayed and then transformed into binary images using Scion imaging software (version 4.0.3., Scion Corp.). The number of binary pixels in the square images was measured automatically. For semi-quantification of fluorescence, five microscopic fields were selected at random, and the number of cells among at least 500 total cells was quantified.

Animals—All animal experimental procedures were approved by the Animal Ethical Committee of Osaka Prefecture University and were performed according to the animal ethical guidelines of Osaka Prefecture University. Male C57BL/6J mice (3 months old, SLC Japan, Shizuoka, Japan) were used for Aβ40 intracerebroventricular (i.c.v.) injection studies. A triple transgenic mouse model of AD (3×Tg-AD), harboring human transgenes of amyloid precursor protein (APP_{SWE}), presenilin-1 ($PS1_{M146V}$), and tau (Tau_{P301L}) under the control of *Thy*1.2 promoters (25), and control mice, were obtained from the Jackson Laboratory (Bar Harbor, ME). Mice of both genders were used at 1, 3, 6, and 9 months of age. All animals were maintained on *ad libitum* ordinary laboratory chow and tap water under a constant 12-h light/12-h dark cycle.

Surgical Procedure—Mice were anesthetized intraperitoneally with sodium pentobarbital (50 mg/kg, intraperitoneally, Abbott) and positioned in a stereotaxic frame (Narishige). The i.c.v. injections of Aβ40 aggregates (50 μM) incubated with or without 10% GAPDH aggregates were administered at a volume of 2 μl using a Hamilton syringe (0.2 μl/min) according to the following coordinates: 0 mm anterior to bregma, 0.8 mm lateral from midline, and 2.2 mm ventral from the skull surface. In this study, animals ($n = 10$) were divided into four treatment groups as follows: 1) control, vehicle, sterilized PBS; 2) aggregated Aβ40 (50 μM) incubated for 48 h at 37 °C in vehicle; 3) aggregated Aβ40 (50 μM) plus 10% GAPDH aggregates (5 μM) in vehicle; and 4) 10% GAPDH aggregates in vehicle. Control and GAPDH siRNA were also injected in 2-μl volumes in the same way.

Hematoxylin and Eosin Staining and Immunohistochemistry—Mice were deeply anesthetized with pentobarbital (200 mg/kg, intraperitoneally) and transcardially perfused with ice-cold PBS followed by 4% paraformaldehyde in PBS. The brain was removed and post-fixed in 4% paraformaldehyde in PBS at 4 °C overnight and then routinely processed and embedded in paraffin. For morphological analysis, paraffin-embedded brain tissues were cut (5 μm thick), deparaffinized, and stained with hematoxylin and eosin. For immunohistochemical analysis, deparaffinized sections were incubated with 100 μg/ml proteinase K (Wako Pure Chemical Industries, Ltd., Osaka, Japan) in 50 mM Tris-HCl buffer (pH 7.4) for 10 min at 37 °C. For detection of Aβ, additional incubation with 70% formic acid for 5 min was performed. After three washes with PBS, sections were incubated with 10% goat serum in PBS, followed by incubation overnight at 4 °C with mouse anti-Aβ monoclonal antibody (6E10, 1:1000), rabbit anti-GAPDH polyclonal antibody (1:500), rabbit anti-AIF polyclonal antibody (1:500), mouse anti-cytochrome *c* monoclonal antibody (1:500), and rabbit anti-GFAP polyclonal antibody (1:1000). Sections were then incubated for 1 h at room temperature with Alexa 488- or Alexa 568-conjugated secondary antibodies, goat anti-rabbit IgG (1:1000), goat anti-mouse IgG (1:1000), and DAPI (1:2000) for nuclear staining and then coverslipped in Fluorescein Mounting Medium (Dako). These antibodies were detected using a confocal scanning microscope (model C1si-TE2000-E, Nikon). For quantification of AIF nuclear translocation, cells exhibiting indication of AIF nuclear translocation were counted and expressed as a ratio to the total number of nuclei stained with DAPI. For quantification of GFAP, cytochrome *c*, Aβ aggregates, and GAPDH aggregates, raw images were first grayed and then transformed into binary images using Scion imaging software (version 4.0.3., Scion Corp.). The number of binary pixels in the square images was measured automatically.

Fractionation and Western Blotting—To detect GAPDH and Aβ aggregates in mice, Triton-insoluble fractions were prepared, and Western blotting was performed as described previously (11). Mouse brains were quickly removed after decapitation, and the hippocampi were dissected. They were then homogenized on ice for 30 s, three times with a sonicator (model Q-125, QSonica LLC, Newton, CT) in tissue lysis buffer containing 150 mM NaCl, 50 mM Tris-HCl (pH 8.0), 1% Nonidet P-40, 10% glycerol, 2 mM PMSF, 1 mM sodium orthovanadate, 10 mM NaF, and protease inhibitor mixture (Roche Diagnostics, Basel, Switzerland). The samples were centrifuged at 15,000 rpm for 10 min at 4 °C. The pellets were resuspended with modified solubilization buffer containing 10 mM HEPES-KOH (pH 7.5), 150 mM NaCl, 0.5% Triton X-100, 1 mM PMSF, 3 mM DTT, and protease inhibitor mixture. The samples were sonicated and then centrifuged at 15,000 rpm for 10 min at 4 °C. The pellets were resuspended with 2× low sample buffer (final concentrations: 62.5 mM Tris-HCl (pH 6.8), 0.5% SDS, and 10% glycerol). Protein concentrations were determined with BCA assays (Pierce). These samples were heated at 100 °C for 5 min, separated by 5–20% SDS-PAGE, and transferred to PVDF membranes (Millipore Japan, Tokyo, Japan). The membrane was incubated for 1 h with Blocking One (Nacalai Tesque, Kyoto, Japan) to block nonspecific binding. The membrane was then incubated overnight at 4 °C with an anti-Aβ monoclonal antibody (1:1000), anti-GAPDH monoclonal antibody (1:300), or anti-H2B polyclonal antibody (1:5000) in 10% Blocking One-PBST (0.05% Tween 20 and 0.02% NaN_3 in PBS) followed by incubation for 1 h at room temperature with a horseradish peroxide-conjugated secondary antibodies (1:5000 anti-mouse for Aβ and GAPDH or anti-rabbit for H2B IgG). Detection was performed using ECL plus and LAS3000 (FUJI-FILM, Tokyo, Japan). Band intensity was measured by Multi Gauge Version 3.0 (FUJI-FILM).

Co-immunoprecipitation—Insoluble fractions prepared from mice hippocampi (0.5 mg/ml, 300 μl) were incubated with normal mouse IgG (2 μg) and 10 μl of 50% protein G-Sepharose slurry (Amersham Biosciences) to pre-clear proteins that bind non-specifically to IgG. After centrifugation (15,000 rpm, 1 min), supernatants were incubated with an anti-Aβ monoclonal antibody (4 μg) overnight at 4 °C, followed by incubation with protein G-Sepharose for 1 h. The beads were washed four times with 1 ml of modified RIPA buffer containing 20 mM Tris-HCl (pH 7.5), 15 mM NaCl, 1 mM EDTA, 1 mM EGTA, 1% Nonidet P-40, 0.1% deoxycholate, 0.1% SDS, 1 mM PMSF, and a protease inhibitor mixture. The beads were added to 40 μl of 2.5× sample buffer followed by incubation for 5 min at 100 °C and Western blotting.

Data Analysis—Data were expressed as mean ± S.D. or S.E. for *in vitro* or *in vivo* studies, respectively, from three or four independent experiments. Statistical analyses were carried out using Student's *t* test and one-way analysis of variance, followed by Dunnett's multiple range test using GraphPad Prism (version 6, GraphPad Software, Inc.). Results with p values <0.05 were considered statistically significant. Complete (100%) amyloidogenesis of Aβ40 was defined as a saturated value of ThT fluorescence obtained from each sample. Time half-values ($t_{½}$) were calculated by sigmoidal curve fitting of the data, using GraphPad Prism (Version 6).

Results

GAPDH Aggregates Accelerate Aβ Amyloidogenesis in Vitro—To validate whether GAPDH aggregates affect Aβ40 amyloidogenesis *in vitro*, we first performed a ThT fluorescence assay (Fig. 1). When Aβ40 was incubated without GAPDH aggregates (*black solid line*), ThT fluorescence of Aβ40 was not detected until day 2 (a lag phase), at which point fluorescence increased from day 3, eventually equilibrating at day 6 (Fig. 1*A*). The $t_{½}$was calculated to be 3.86 ± 0.06 days. Aβ40 incubation with 10% GAPDH aggregates resulted in a ThT fluorescence curve that increased hyperbolically without a lag phase, equilibrating at day 2 (Fig. 1*A*, *dotted line*); $t_{½}$ was 1.16 ± 0.07 days. The degree of the leftward shift was ~3-fold. In the following studies, we examined samples at day 2, when we observed the largest differences between treatment with Aβ40 with and without 10% GAPDH aggregates. GAPDH aggregates enhanced ThT fluorescence of Aβ40 in a concentration-dependent manner (by ~10-, 25-, or 40-fold with the addition of 0.1, 1, or 10% GAPDH aggregates, respectively); ThT fluorescence in the solution of 10% GAPDH aggregates was not observed (Fig. 1*B*). Furthermore, addition of native GAPDH, instead of aggregated GAPDH, did not

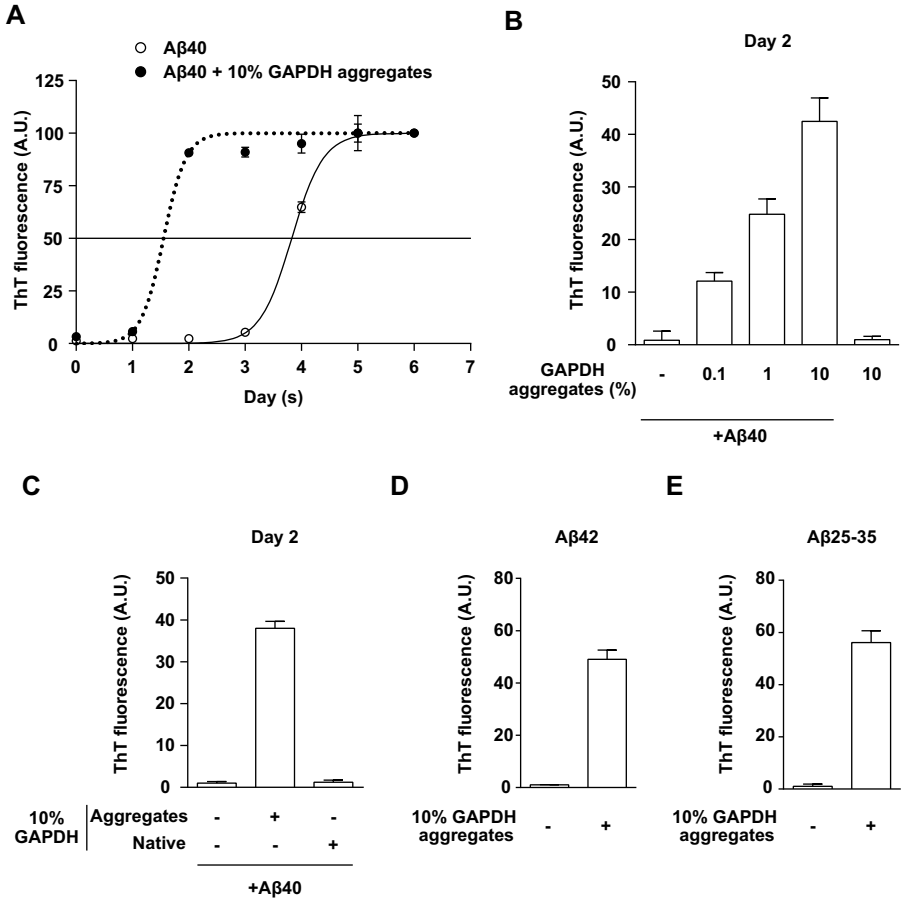

FIGURE 1. **GAPDH aggregates accelerate Aβ40 amyloidogenesis *in vitro*.** *A,* effect of 10% (5 μM) GAPDH aggregates on Aβ40 (50 μM) amyloidogenesis. ThT fluorescence of Aβ40 alone (*solid black line with open circles*) and Aβ40 incubated with GAPDH aggregates (*dotted black line* with *closed circles*) was measured at the indicated time points. *B,* concentration-dependent effects of 0.1, 1, and 10% GAPDH aggregates (0.05, 0.5, and 5 μM, respectively) on ThT fluorescence of Aβ40 were measured on day 2. The fluorescence of 10% GAPDH aggregates alone was measured in the same manner. *C,* effect of native (non-aggregated) GAPDH (5 μM) on ThT fluorescence of Aβ40 was measured on day 2. Data are presented as mean ± S.D. of four independent experiments. Effects of 10% GAPDH aggregates on Aβ42 (*D*) and Aβ(25–35) (*E*) amyloidogenesis. Aβ42 (25 μM) or Aβ(25–35) (50 μM) was incubated without or with 10% GAPDH aggregates for 1 h before ThT fluorescence was measured. Data are the mean ± S.D. of four independent experiments. *A.U.*, arbitrary units.

enhance ThT fluorescence; there was also no enhancement of fluorescence when Aβ40 was incubated alone (Fig. 1*C*). Similarly, Aβ42 and Aβ(25–35), which are known to be more prone to aggregation compared with Aβ40, were incubated with GAPDH aggregates for 1 h to demonstrate augmentation of ThT fluorescence (Fig. 1, *D* and *E*). Incubation of Aβ40 with 10% aggregates of bovine serum albumin did not affect ThT fluorescence (data not shown). These results suggest that GAPDH aggregation specifically augments Aβ amyloidogenesis.

Structural Changes in Aβ40 Incubated with GAPDH Aggregates—We next examined Aβ40 birefringence stained with Congo red, considered to be one of the most reliable methods for determination of amyloid structure (41). Aβ40 incubated with or without 10% GAPDH aggregates was confirmed to bind Congo red under non-polarized light (Fig. 2*A*, *panels a* and *b*). Although Aβ40 alone did not show any birefringence under polarized light (Fig. 2*A*, *panel c*), Aβ40 incubated with 10% GAPDH aggregates displayed prominent apple-green birefringence (Fig. 2*A*, *white arrow* in *panel d*).

β-Sheet secondary structure is a common feature of proteins undergoing amyloidogenesis (42, 43). Thus, the amount of protein with β-sheet structure in samples of Aβ40 incubated with or without GAPDH aggregates was analyzed using CD spectra in the far-ultraviolet region (200–250 nm, Fig. 2*B*). The spectra of Aβ40 incubated alone and fresh Aβ40 (without incubation) had minimums under 200 nm and were characteristic of random coil conformation (Fig. 2*B, black solid line* and *black dashed line*, respectively). In contrast, the spectra of Aβ40 incubated with 0.1 and 1% GAPDH aggregates had increased negative ellipticities at 209 and 216 nm (Fig. 2*B, red* and *green solid line*s), respectively. Furthermore, the spectrum of Aβ40 incubated with 10% GAPDH aggregates displayed a minimum at ~218 nm, a feature indicative of a predominantly β-sheet conformation (Fig. 2*B, blue solid line*) (44). These results demonstrate that GAPDH aggregates increase the amount of Aβ40 with a β-sheet structure in a concentration-dependent manner.

We further examined the morphology of Aβ40 incubated with or without 0.1, 1, or 10% GAPDH aggregates using AFM. Aβ40 incubated without GAPDH aggregates was represented by numerous unassembled species and did not display typical amyloidal fibrillar structure (Fig. 2*C*, *panel a*). When Aβ40 was incubated with 0.1% GAPDH aggregates, typical amyloid fibrils were observed (Fig. 2*C*, *white arrows* in *panel b*). These fibrils

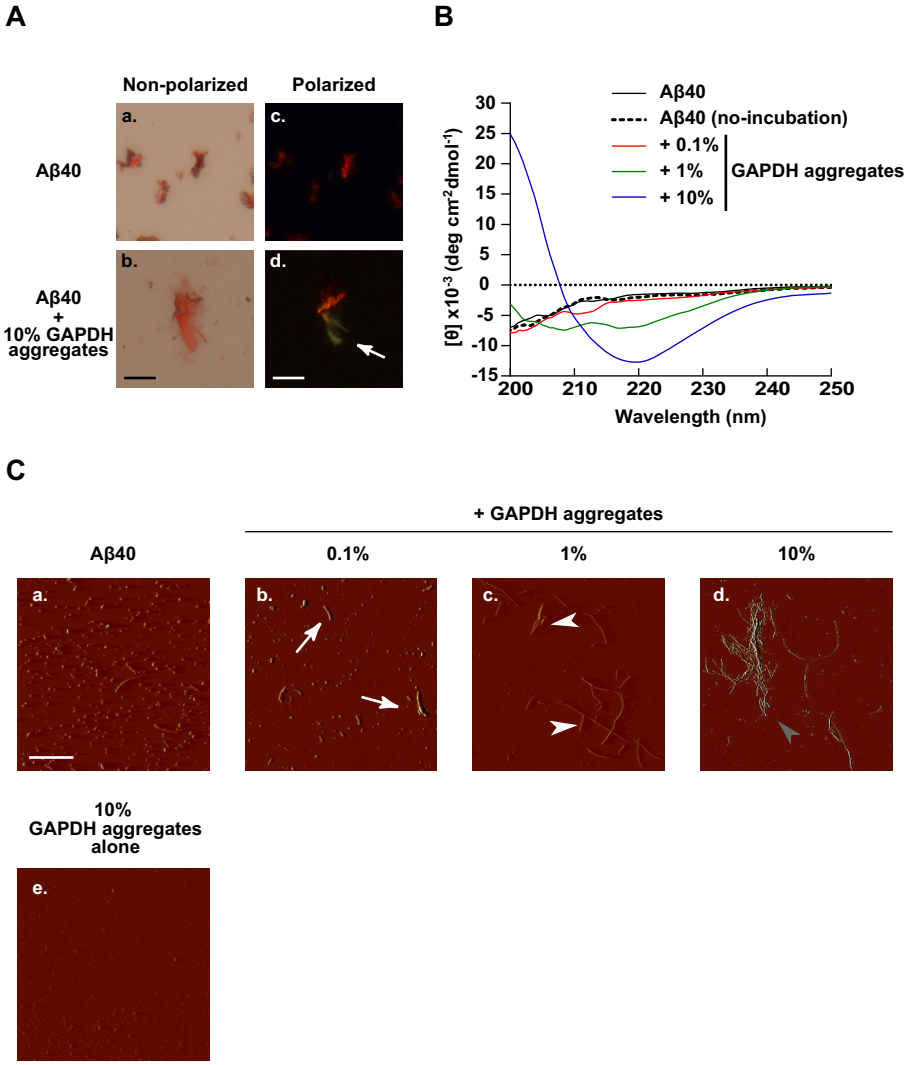

FIGURE 2. **Structural changes in Aβ40 incubated with GAPDH aggregates.** *A,* Congo red birefringence was measured. *Panels a* and *b* show images captured under non-polarized light, and *panels c* and *d* show images captured under polarized light. Birefringence was observed in Aβ40 (50 μM) incubated with 10% (5 μM) GAPDH aggregates for 2 days, as indicated by the *white arrow*. *Scale bars,* 10 μm. *B,* far-ultraviolet CD spectra of Aβ40 with or without GAPDH aggregates (0.1, 1, and 10%). The *solid lines* (*black, red, green,* and *blue*) represent CD spectra of Aβ40 incubated with or without GAPDH aggregates for 2 days, and the *dotted black line* represents CD spectrum of Aβ40 at day 0 (*no incubation*). *C,* AFM images of Aβ40 incubated for 2 days with or without (*panel a*) GAPDH aggregates (*panels b–d* show Aβ40 with 0.1, 1, 10% GAPDH, respectively) or 10% GAPDH aggregates alone (*panel e*). *Scale bar,* 2 μm.

were elongated when Aβ40 was incubated with 1% GAPDH aggregates (Fig. 2*C*, *white arrowheads* in *panel c*). When Aβ40 was incubated with 10% GAPDH aggregates, we observed assemblies of these elongated amyloid fibrils (Fig. 2*C*, *gray arrowhead* in *panel d*). We did not observe any of these structures in 10% GAPDH aggregates incubated alone (Fig. 2*C*, *panel e*). These data indicate that GAPDH aggregates can substantially alter Aβ40 morphology in a concentration-dependent manner.

GAPDH Aggregates Potentiate Aβ40-induced Cytotoxicity in PC12 Cells, Concomitant with Mitochondrial Dysfunction—We next examined whether augmentation of Aβ40 amyloidogenesis by GAPDH aggregates influences PC12 cell viability (Fig. 3*A*). Cell viability significantly decreased by 28% ($p < 0.05$) in cells treated with 50 μM Aβ alone compared with vehicle-treated controls. Treatment with Aβ40 co-incubated with GAPDH aggregates further decreased cell viability in a concentration-dependent manner, decreasing by 58% ($p < 0.05$) or 78% ($p < 0.01$) when Aβ40 was incubated with 1 or 10% GAPDH aggregates, respectively. Treatment with 10% GAPDH aggregates alone did not decrease cell viability, compared with vehicle-treated controls (Fig. 3*A*).

To investigate mechanisms enhancing Aβ40-induced cell death by GAPDH aggregates, we next investigated mitochondrial dysfunction, which is known to play a key role in the pathogenesis of AD (32). Mitochondrial membrane potential was measured as an index of mitochondrial dysfunction (45) using rhodamine 123, a marker of mitochondrial membrane potential (Fig. 3*B*). Treatment with Aβ40 incubated alone did not increase rhodamine fluorescence (Fig. 3*B*, *panels a* and *b*). In contrast, treatment with Aβ40 incubated with 10% GAPDH aggregates significantly increased rhodamine fluorescence by ~1.7-fold, indicating disruption of mitochondrial membrane potential (Fig. 3*B*, *panel c*). Treatment with 10% GAPDH alone did not change rhodamine fluorescence (Fig. 3*B*, *panel d*). These results suggest that GAPDH aggre-

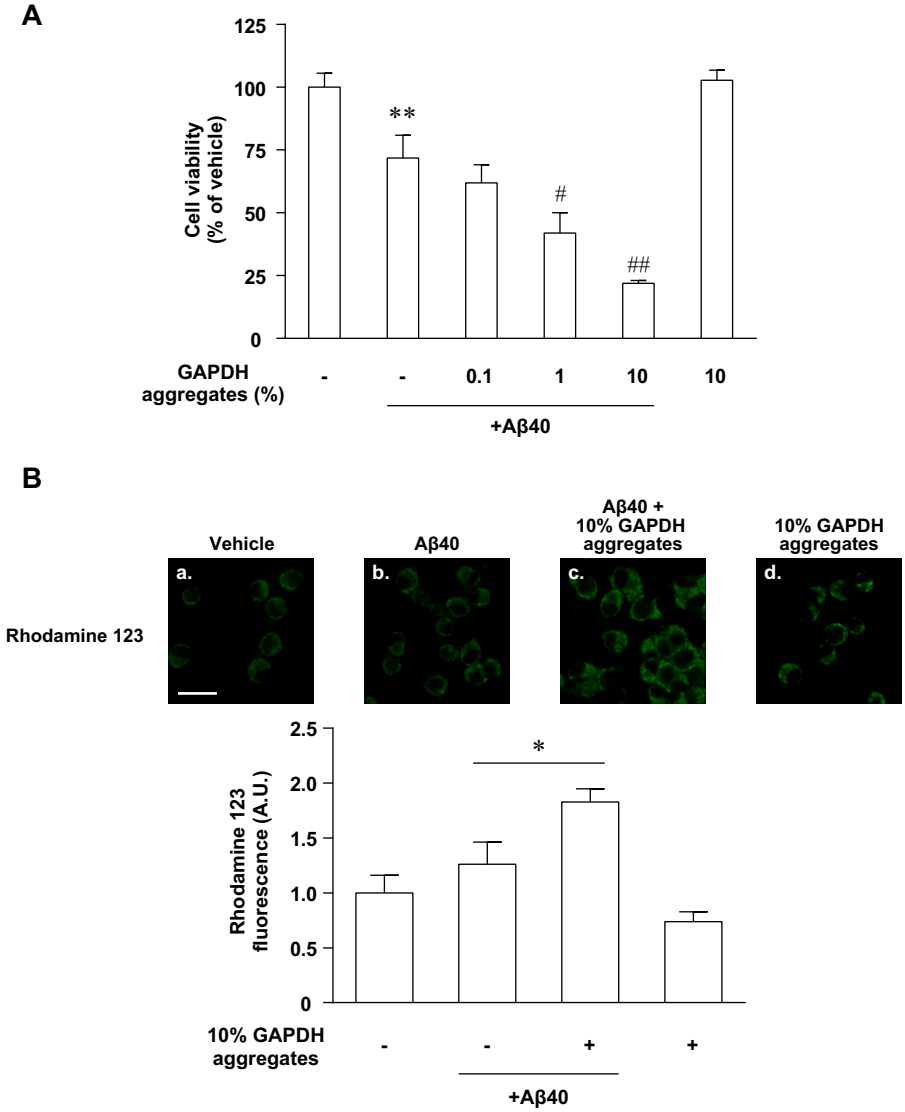

FIGURE 3. **GAPDH aggregates potentiate Aβ40-induced cytotoxicity in PC12 cells, concomitant with mitochondrial dysfunction.** *A*, cell viability of PC12 cells was measured 72 h after treatment with Aβ40 incubated with GAPDH aggregates. Data are presented as mean ± S.D. of four independent experiments (**, $p < 0.01$, relative to control, as determined by Student's *t* test; #, $p < 0.05$; ##, $p < 0.01$, relative to 50 μM Aβ40, as determined by Dunnett's multiple range test). *B*, mitochondrial membrane potential was assessed using the fluorescent dye, rhodamine 123 (*panels a–d* show treatment with vehicle, Aβ40 incubated alone, Aβ40 incubated with 10% GAPDH aggregates, and 10% GAPDH aggregates alone, respectively). Distribution of the fluorescent signal was measured automatically using Scion imaging software. Data are presented as mean ± S.D. of four independent experiments (*, $p < 0.05$, relative to 50 μM Aβ40, as determined by Student's *t* test). *A.U.*, arbitrary units. *Scale bar*, 10 μm.

gates enhance Aβ40-induced cell death via mitochondrial dysfunction.

GAPDH Aggregates Potentiate Aβ40-induced Neurotoxicity in Vivo—To examine the effect of GAPDH aggregates on Aβ40-induced neurotoxicity *in vivo*, i.c.v. injections of Aβ40 incubated with or without 10% GAPDH aggregates were administered (Fig. 4*A*). In C57BL/6J mice treated with Aβ40 incubated alone, pyramidal cells in the hippocampal CA3 region with pyknotic nuclei increased in number to a maximum of ~2.5-fold (Fig. 4*B*, *panel b*), compared with vehicle-treated mice (Fig. 4*B*, *panel a*). The number of such pathological cells was counted and graphed (Fig. 4*B*, *right panel*). Treatment with Aβ40 incubated with 10% GAPDH aggregates significantly increased the number of cells with pyknotic nuclei by ~2.2-fold, compared with mice treated with Aβ40 incubated alone ($p < 0.05$, Fig. 4*B*, *panel c*). In contrast, when mice were i.c.v.-injected with 10% GAPDH aggregates alone, the resultant number of pathological cells was almost identical to that of the vehicle-treated group (Fig. 4*B*, *panel d*). Consistent with previous reports showing the vulnerability of the hippocampal CA3 region to Aβ toxicity (46, 47), these pathological changes were not observed in any other brain areas (data not shown).

We next examined astrocyte accumulation using GFAP immunohistochemistry (Fig. 4*C*), which is considered to be an index of pathological gliosis in AD (48). The amount of detected GFAP in mice treated with Aβ40 alone increased significantly by ~1.8-fold compared with vehicle-treated mice ($p < 0.05$, Fig. 4*C*, *panel b*). The amount of detected GFAP after treatment with Aβ40 incubated with 10% GAPDH aggregates was further elevated by ~2.5-fold ($p < 0.01$, Fig. 4*C*, *panels b* and *c*), compared with mice treated with Aβ40 alone. We did not observe any difference in results after treatment with vehicle or 10%

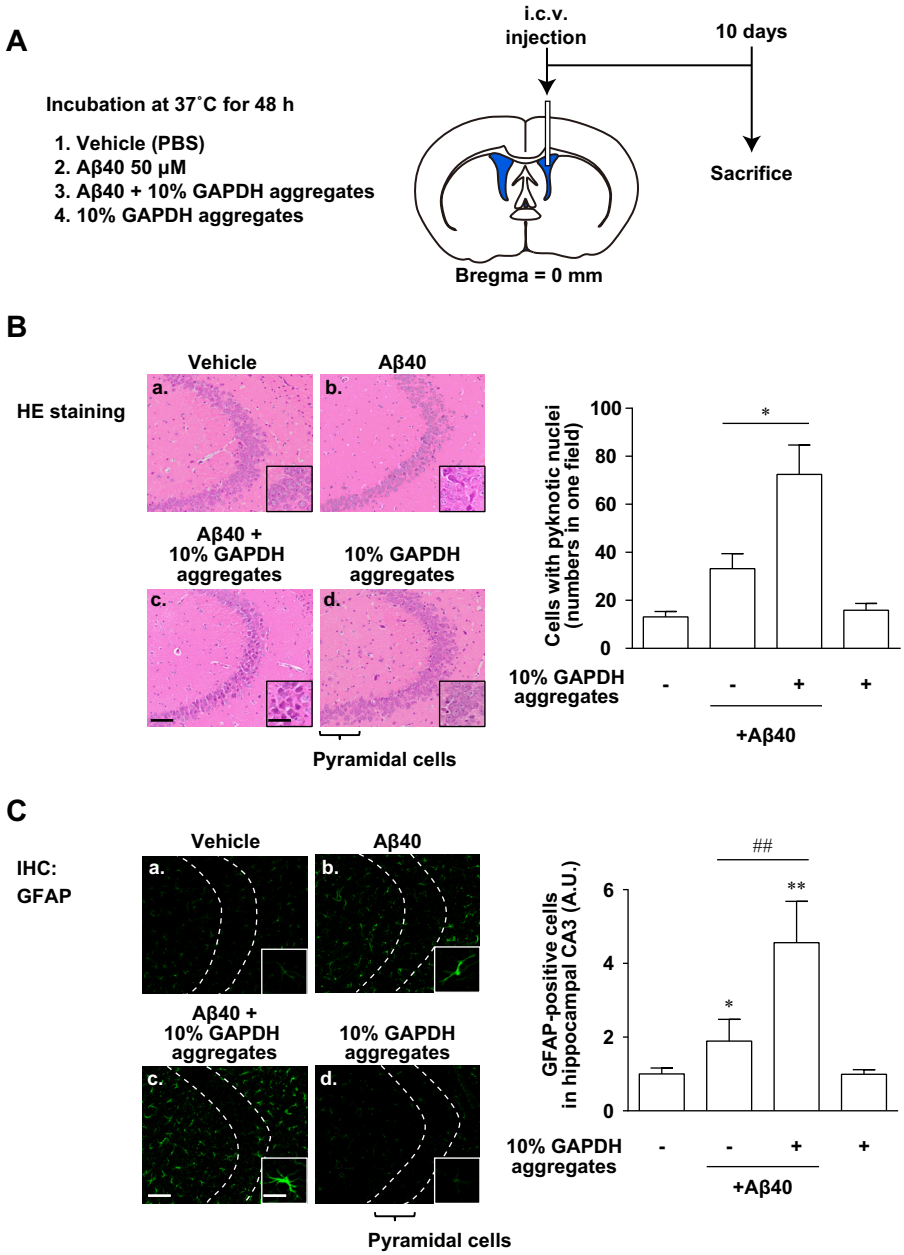

FIGURE 4. **GAPDH aggregates potentiate Aβ40-induced neurotoxicity *in vivo*.** *A*, study design and experimental scheme. Solutions containing Aβ40 with or without GAPDH aggregates were incubated at 37 °C for 48 h and then injected i.c.v. Ten days after i.c.v. injection, mice were sacrificed and subjected to the following experiments. *B*, hematoxylin and eosin staining of the hippocampal CA3 region (*left panels*; *panels a–d* show treatment with vehicle, Aβ40 incubated alone, Aβ40 incubated with 10% GAPDH aggregates, and 10% GAPDH aggregates alone, respectively). The number of pyknotic cells was counted manually (*right panel*). Data are presented as mean ± S.E. of four independent experiments (*, $p < 0.05$, relative to Aβ40 treatment, as determined by Student's *t* test). *Scale bar*, 100 μm. Magnification of selected portions of images are shown in the *insets*. *Scale bar*, 25 μm. *C*, immunohistochemistry (*IHC*) targeting GFAP in the hippocampal CA3 region (*panels a–d* show treatment with vehicle, Aβ40 incubated alone, Aβ40 incubated with 10% GAPDH aggregates, and 10% GAPDH aggregates alone, respectively). Fluorescence intensity was measured automatically using Scion imaging software. Data are presented as mean ± S.E. of four independent experiments (*, $p < 0.05$; **, $p < 0.01$, relative to vehicle treatment, as determined by one-way analysis of variance, followed by Dunnett's multiple range test; ##, $p < 0.01$, relative to Aβ40 treatment, as determined by Student's *t* test). *A.U.*, arbitrary units. *Scale bar*, 100 μm. Magnification of selected portions of images are shown in the *insets*. *Scale bar*, 25 μm.

GAPDH aggregates alone (Fig. 4*C*, *panels a* and *d*). These immunohistochemistry results are quantified in the graph in Fig. 4*C* (*right panel*) Together, these results suggest that GAPDH aggregates might be associated with AD pathogenesis.

GAPDH Aggregates Enhance Aβ40-induced Mitochondrial Dysfunction in Vivo—To investigate mechanisms underlying the enhancement of Aβ40-induced neurotoxicity by GAPDH aggregates, we performed immunohistochemical studies on AIF and cytochrome *c* (Fig. 5), which are established markers of mitochondrial dysfunction (49). The number of pyramidal cells in the hippocampal CA3 region exhibiting AIF nuclear translocation was counted (Fig. 5*A*). AIF was predominantly localized to the cytosol of mice treated with vehicle (Fig. 5*A*, *panels a* and *e*). Approximately 7% of cells showed AIF nuclear translocation after treatment with Aβ40 alone (Fig. 5*A*, *panels b* and *f*). The number of cells displaying AIF nuclear translocation signifi-

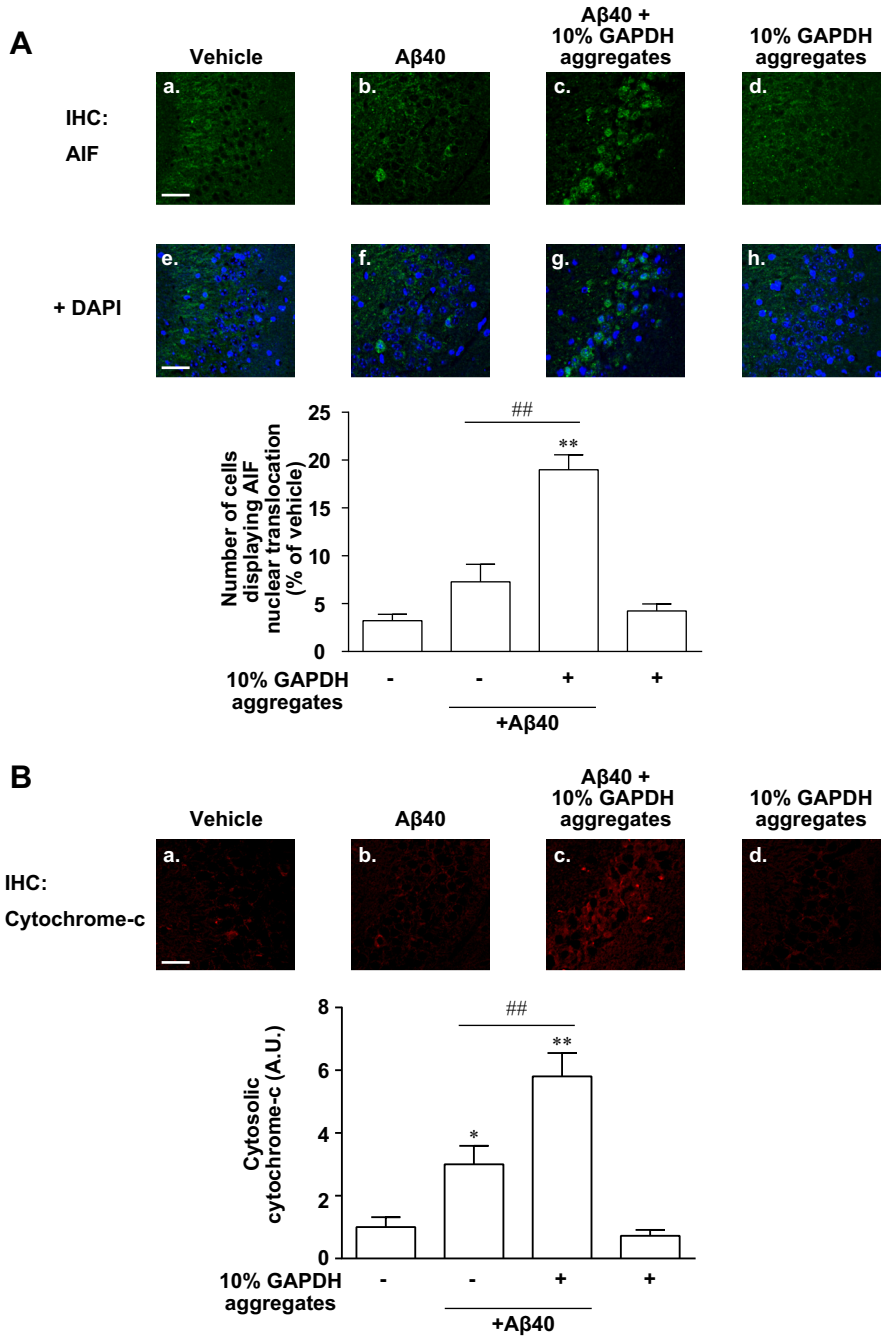

FIGURE 5. **GAPDH aggregates enhance Aβ40-induced mitochondrial dysfunction *in vivo*.** Solutions containing Aβ40 with or without GAPDH aggregates were incubated at 37 °C for 48 h and injected i.c.v. Ten days after i.c.v. injection, mice were sacrificed and subjected to the following experiments. *A,* immunohistochemistry (*IHC*) targeting AIF was performed (*panels a–d* show treatment with vehicle, Aβ40 incubated alone, Aβ40 incubated with 10% GAPDH aggregates, and 10% GAPDH aggregates alone, respectively; corresponding images merged with nuclear staining (+ *DAPI*) are shown in *panels e–h*, respectively). The number of cells displaying nuclear translocation of AIF was counted manually (*upper graph*). Data are presented as mean ± S.E. of four independent experiments (**, $p < 0.01$, relative to vehicle treatment, as determined by one-way analysis of variance, followed by Dunnett's multiple range test; ##, $p < 0.01$, relative to Aβ40 treatment, as determined by Student's *t* test). *Scale bars,* 20 μm. *B,* immunohistochemistry targeting cytochrome *c* was performed (*panels a–d* show treatment with vehicle, Aβ40 incubated alone, Aβ40 incubated with 10% GAPDH aggregates, and 10% GAPDH aggregates alone, respectively), and the release of cytochrome *c* to the cytosol was quantified using densitometry (*lower graph*). Data are presented as mean ± S.E. of four independent experiments (*, $p < 0.05$; **, $p < 0.01$, relative to vehicle treatment, as determined by one-way analysis of variance, followed by Dunnett's multiple range test; ##, $p < 0.01$, relative to Aβ40 treatment, as determined by Student's *t* test). *Scale bar,* 20 μm.

cantly increased by ~18% after treatment with Aβ40 incubated with 10% GAPDH aggregates compared with Aβ40 alone (Fig. 5*A*, *panels c* and *g*). Treatment with 10% GAPDH aggregates alone did not affect AIF nuclear translocation (Fig. 5*A*, *panels d* and *h*).

Detection of cytochrome *c*, the punctate signals of which indicate localization of cytochrome *c* to mitochondria, was observed in vehicle-treated mice (Fig. 5*B*, *panel a*). After treatment with Aβ40 alone, the signal had a less punctate pattern and was widely distributed in the cytosol (Fig. 5*B*, *panel b*) by

~3-fold ($p < 0.05$), compared with vehicle-treated mice, indicating the release of cytochrome c from mitochondria. This change in signal distribution was more marked after treatment with Aβ40 incubated with 10% GAPDH aggregates (Fig. 5*B*, *panel c*) by maximal degree to ~5.8-fold ($p < 0.01$). There was no change in cytochrome *c* signal distribution in mice treated with vehicle or 10% GAPDH aggregates alone (Fig. 5*B*, *panel d*). These results suggest that GAPDH aggregates likely enhance Aβ40-induced mitochondrial dysfunction in the context of AD.

GAPDH Aggregates Accelerate Aβ40 Amyloidogenesis and Potentiate Aβ Toxicity—These results raised the question of whether GAPDH aggregates merely accelerate Aβ40 amyloidogenesis or whether they also increase Aβ40 toxicity. To clarify this point, Aβ40 incubated alone for 6 days and Aβ40 incubated with GAPDH aggregates for 2 days with similar levels of Aβ40 amyloidogenesis (assessed by ThT fluorescence, Figs. 1*A* and 6*A*) were used for i.c.v. injection. In mice treated with Aβ40 incubated with GAPDH aggregates for 2 days, cells with pyknotic nuclei were significantly more numerous than in mice treated with Aβ40 incubated for 6 days (Fig. 6*B*). Similarly, the number of GFAP-positive cells was higher in mice treated with Aβ40 incubated with GAPDH aggregates for 2 days compared with mice treated with Aβ40 incubated for 6 days (Fig. 6*C*). These results indicate that GAPDH aggregates both accelerate Aβ40 amyloidogenesis and potentiate Aβ40 neurotoxicity.

Co-localization of GAPDH Aggregates with Aβ Aggregates in the Cortex and Hippocampal CA3 Region of 3×Tg-AD Mice—To further investigate potential association between GAPDH aggregates and Aβ in AD pathogenesis, we used 3×Tg-AD mice for immunohistochemical analysis of Aβ and GAPDH in the brain. The brain regions analyzed are shown as *red squares*, indicating the cortex and hippocampal CA3 region (Fig. 7*A*). In 9-month-old 3×Tg-AD mice, immunostaining revealed extracellular deposits of Aβ in the cortex, consistent with senile plaques in human AD. These deposits were also positive for GAPDH (Fig. 7*B*), indicating co-localization of GAPDH and Aβ. In contrast to the control mice, in 3-month-old 3×Tg-AD mice, but not 1-month-old mice, hippocampal CA3 pyramidal neurons exhibited punctate Aβ-positive signals, which were more abundant at 6 months of age (Fig. 7*C*). These findings have been confirmed by several groups to be age-dependent Aβ aggregation (25, 50). We also observed punctate GAPDH signaling in control and 3×Tg-AD mice as early as 1 month of age, which increased at 3 and 6 months of age (Fig. 7*C*). Furthermore, GAPDH-positive and Aβ-positive signals partially co-localized in 3×Tg-AD mice that were 3 and 6-months old (Fig. 7*C*). These results were quantified in the *graph* in Fig. 7*D*. Thus, these data suggest that GAPDH aggregation occurs prior to Aβ aggregation.

We further investigated whether these GAPDH- and Aβ-positive signals were related to mitochondrial dysfunction in 6-month-old 3×Tg-AD mice (Fig. 7*E*). Consistent with our data from i.c.v.-injected mice, AIF nuclear translocation and cytochrome *c* release were observed in pyramidal cells of the hippocampal CA3 region (Fig. 7*E*). Collectively, these results suggest that in 3×Tg-AD mice, GAPDH aggregates co-localize with Aβ aggregates both extracellularly and intracellularly and that GAPDH aggregation precedes Aβ aggregation in the hippocampal CA3 region, leading to mitochondrial dysfunction.

GAPDH and Aβ Aggregates Interact and Enhance Aβ Aggregation in 3×Tg-AD Mice—To examine the interaction between GAPDH and Aβ aggregates, we next performed a co-immunoprecipitation assay using both insoluble fractions from the hippocampi of 3-month-old 3×Tg-AD mice and an anti-Aβ antibody. The result revealed a clear interaction between GAPDH and Aβ in insoluble fractions (Fig. 8).

Finally, to investigate the pathophysiologic significance of GAPDH aggregates on Aβ aggregation in AD pathogenesis, we conducted experiments using GAPDH silencing and supplementary methods. The 3×Tg-AD mice were i.c.v. injected with either GAPDH siRNA or GAPDH aggregates, and each insoluble fraction from the hippocampus collected 10 days after injection was subjected to Western blotting using an anti-Aβ antibody (Fig. 9*A*). In mice treated with control siRNA, numerous Aβ-positive signals (*i.e.* Aβ aggregates) were detected. In contrast, these Aβ aggregates were significantly reduced by approximately half in GAPDH siRNA-treated mice (Fig. 9*B*). Conversely, Aβ aggregates were increased by ~1.2-fold in GAPDH aggregate-injected mice compared with vehicle-treated mice (Fig. 9*C*). These results indicate that GAPDH aggregates enhance Aβ aggregate formation in 3×Tg-AD mice.

Discussion

This study demonstrates that GAPDH aggregates enhance Aβ40 amyloidogenesis, as determined by ThT fluorescence, Congo red birefringence, and far-ultraviolet CD spectra; our AFM studies also revealed that GAPDH aggregates markedly change the morphology of Aβ40 (Figs. 1 and 2). Moreover, augmentation of Aβ40 amyloidogenesis by GAPDH aggregates potentiated Aβ40-induced neurotoxicity, accompanied by mitochondrial dysfunction *in vitro* and *in vivo* (Figs. 3–6). Concomitant with mitochondrial dysfunction, GAPDH aggregates were also found to co-localize with extracellular and intracellular Aβ aggregates in aged 3×Tg-AD mice (Fig. 7). Furthermore, we demonstrated an interaction between GAPDH and Aβ aggregates (Fig. 8), and we showed that GAPDH aggregates enhance Aβ aggregate formation in 3×Tg-AD mice (Fig. 9). These results support our hypothesis. GAPDH aggregates accelerate Aβ amyloidogenesis and may, at least in part, contribute to AD pathogenesis (Fig. 10, hypothetical working model).

GAPDH aggregates are likely involved in the initiation and progression of AD pathogenesis. It is generally accepted that Aβ amyloidogenesis leads to increases in the oligomers and fibrils that play a central role in the initiation and progression of AD (24). The concentration of Aβ *in vivo* is reported to be ~5 nM (51, 52), whereas aggregation *in vitro* requires a concentration nearly 3 orders of magnitude greater than *in vivo* values (53). To account for this discrepancy, the "seeding" hypothesis has been proposed, based on nucleation-dependent protein polymerization, (54). The seeding hypothesis proposes that a number of lipids and proteins, such as GM1 ganglioside and Aβ42, serve as "seeds" for Aβ40 (55). The sigmoidal curve of our ThT fluorescence data, demonstrating that incubation of Aβ40 with GAPDH aggregates increases ThT fluorescence in a concentration-dependent manner, is consistent with a

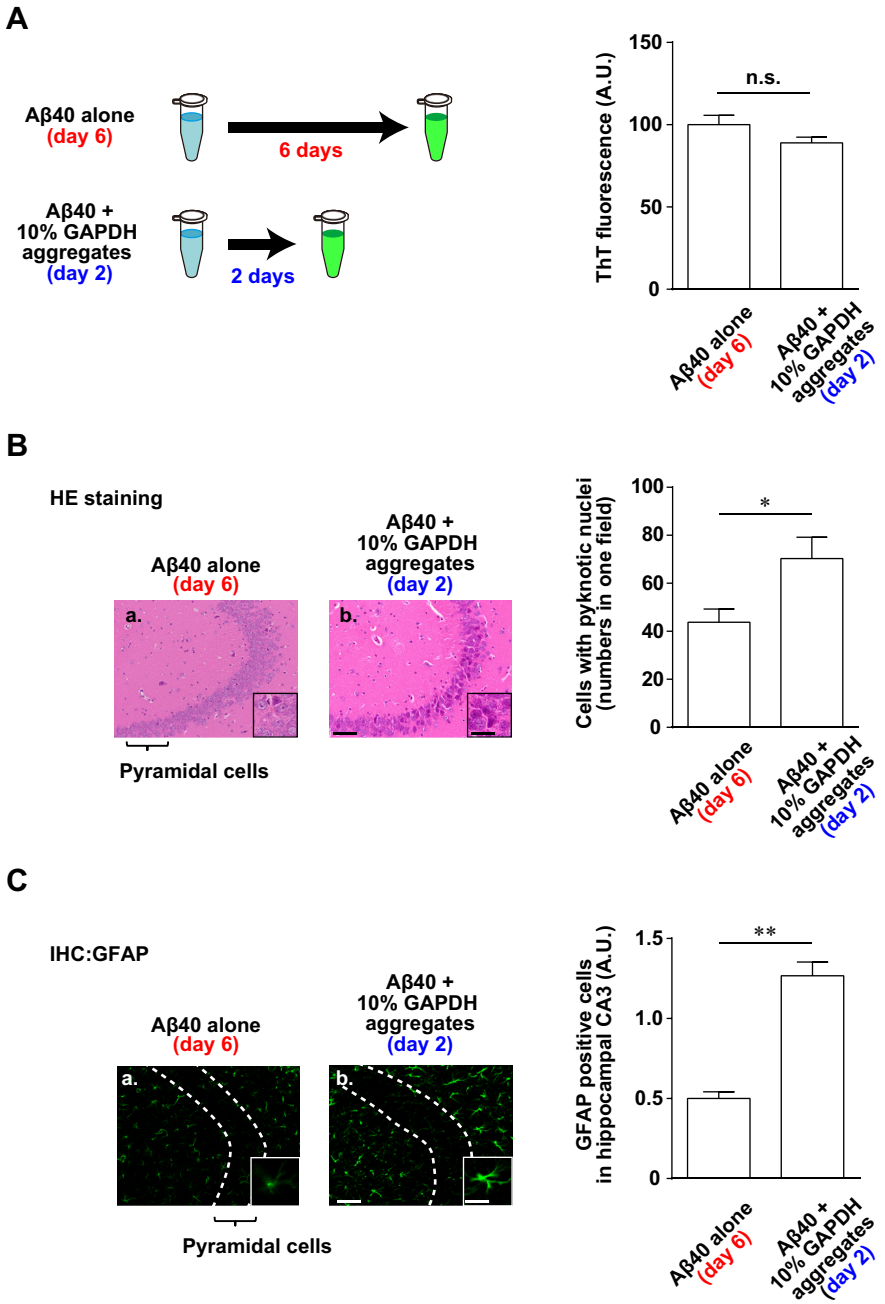

FIGURE 6. **GAPDH/Aβ co-aggregates are highly toxic compared with Aβ40 fibrils.** *A,* Aβ40 was incubated either alone for 6 days or with GAPDH aggregates for 2 days before ThT fluorescence was measured. Mice were i.c.v. injected with these incubated Aβ40 samples and subjected to experiments at day 10 (as described in Fig. 4). *n.s.*, no significance. *B,* hematoxylin and eosin staining in the hippocampal CA3 region (*panels a* and *b* show images from animals treated with Aβ40 incubated alone for 6 days and Aβ40 incubated with 10% GAPDH aggregates for 2 days, respectively). The number of pyknotic cells was counted manually. Data are the mean ± S.E. of four independent experiments (*, $p < 0.05$, relative to treatment with Aβ40 incubated alone for 6 days, Student's *t* test). *Scale bar,* 100 μm. Magnifications of selected portions of the images are shown in the *insets*. *Scale bar,* 25 μm. *C,* GFAP immunohistochemistry (*IHC*) in the CA3 region (*a* and *b* show images from animals treated with Aβ40 incubated alone for 6 days and Aβ40 incubated with 10% GAPDH aggregates for 2 days, respectively). The fluorescence intensity was automatically measured using Scion image software. Data are the mean ± S.E. of four independent experiments (**, $p < 0.01$, relative to the treatment with Aβ40 incubated alone for 6 days, Student's *t* test). *Scale bar,* 100 μm. *A.U.*, arbitrary units. Magnifications of selected portions of the images are shown in the *insets*. *Scale bar,* 25 μm.

nucleation-dependent polymerization model of Aβ40 amyloidogenesis (54). We further show that co-incubation with GAPDH aggregates, but not soluble forms of GAPDH, specifically enhanced Aβ40 amyloidogenesis (Figs. 1 and 2). GAPDH aggregates also potentiated the amyloidogenesis of Aβ42 and Aβ(25–35) (Fig. 1, *D* and *E*), which are known to aggregate more quickly and act as "seeds" for Aβ40, contributing to greater neurotoxicity. However, "seed" has been defined as an aggregation-inducing factor leading to immediate polymerization without any lag time (54). Therefore, GAPDH aggregates cannot be strictly defined as seeds due to their lag time (Fig. 1*A*). These observations raise the possibility that GAPDH aggregation instead serves as an accelerator of Aβ nucleation, which is the rate-limiting step in Aβ aggregation.

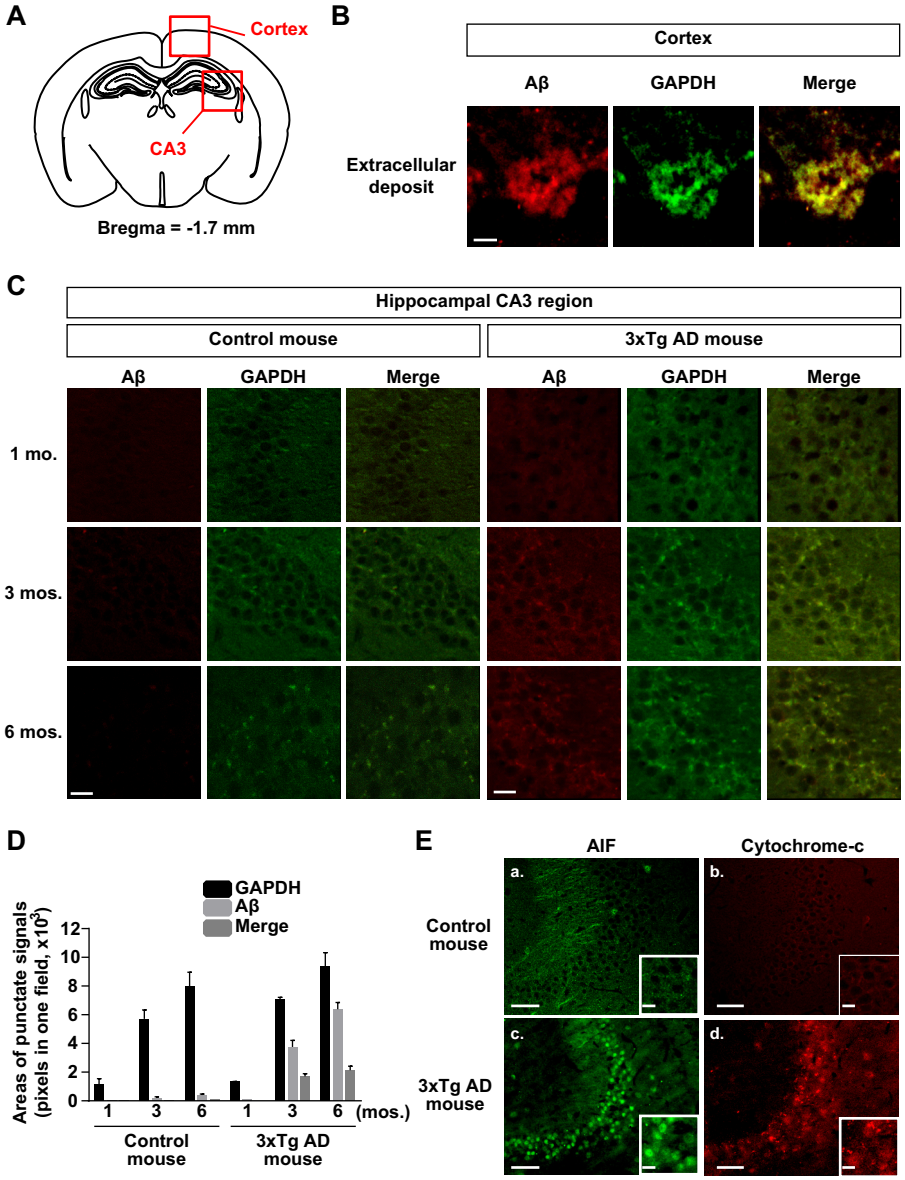

FIGURE 7. **Co-localization of GAPDH aggregates with Aβ aggregates in cortical and the hippocampal CA3 regions of 3×Tg-AD mice.** *A,* schema indicating cortical and hippocampal CA3 regions investigated in the following experiments. *B,* double immunofluorescence staining of Aβ and GAPDH showing co-localization in extracellular deposits. *Scale bar,* 20 μm. *C,* Aβ and GAPDH aggregation increased in an age-dependent manner and co-localized in pyramidal cells of the hippocampal CA3 region. *Scale bar,* 20 μm. *D,* number of punctate signals (*Aβ*, *GAPDH*, and *merge*) was measured automatically using Scion imaging software. Data are presented as mean ± S.E. of three independent experiments. *E,* immunofluorescence staining for AIF (*panel a*, control mouse; *panel c,* 3×Tg-AD mouse) and cytochrome *c* (*panel b*, control mouse; *panel d*, 3×Tg-AD mouse). Nuclear translocation of AIF and release of cytochrome *c* were observed in pyramidal cells in the hippocampal CA3 region of 6-month-old control and 3×Tg-AD mice. *Scale bars,* 50 μm. Magnification of selected portions of images are shown in the *insets*. *Scale bars,* 10 μm.

This study suggests that GAPDH aggregates enhance Aβ40-induced cell death *in vitro* and *in vivo* (Figs. 3 and 4), as a result of increases in β-sheet content in Aβ40 aggregates (Figs. 1 and 2). Identification of the species specifically causing neurodegeneration is currently one of the most controversial topics in the field of AD research. It is not clear whether fibrils (38, 56) or soluble oligomers (57, 58) have more serious toxicity responsible for AD pathology. However, there is a growing number of reports supporting the idea that the disease-associated, aggregation-prone protein readily adopts a β-sheet secondary structure (42, 43) and that the ability to form β-sheet secondary structures is important for determining toxicity (59, 60). Therefore, GAPDH aggregates may facilitate the conversion of Aβ to a more toxic species by increasing β-sheet content. In addition to the β-sheet contents, the concern regarding polymorphisms affecting Aβ fibril toxicity has been growing. An example of a polymorphism having such an effect is that GM1 ganglioside not only accelerates Aβ aggregation, it also changes Aβ fibril conformation and enhances toxicity (61). Taking this into account, our results show that GAPDH aggregates accelerate Aβ40 amyloidogenesis and also potentiate that Aβ40 neurotoxicity (Fig. 6) is attributed to the formation of highly toxic materials.

Our results indicate that co-incubation of Aβ40 with GAPDH aggregates might have caused significant mitochondrial dysfunction (Figs. 3*B* and 5). This dysfunction occurred

alongside enhancement of Aβ40 neurotoxicity by GAPDH aggregates (Figs. 3*A* and 4). It has been reported that extracellular and intracellular Aβ aggregation in AD induced disruption of mitochondrial membrane potential (30, 31). In this study, i.c.v. injections of Aβ40 co-incubated with GAPDH aggregates led to nuclear translocation of AIF and cytoplasmic release of cytochrome *c* from mitochondria, which was also observed in 6-month-old 3×Tg-AD mice (Figs. 5 and 7*E*). AIF nuclear translocation activates endonuclease-G in a caspase-independent manner, and released cytochrome *c* initiates caspase-dependent cell death (32). Consequently, these events lead to neuronal cell death (32). Therefore, Aβ40 co-incubation with GAPDH aggregates likely specifically triggers mitochondrial dysfunction, because Aβ40 aggregates alone did not disrupt mitochondrial membrane potential (Figs. 3*B* and 5). Moreover, taking into account the fact that control mice did exhibit the mitochondrial dysfunction observed in 3×Tg mice (Fig. 7*E*), these apoptotic changes are likely attributable to Aβ toxicity.

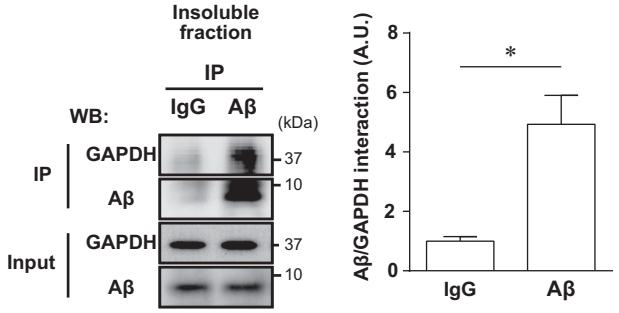

FIGURE 8. **GAPDH aggregates interact with Aβ aggregates in the 3×Tg-AD mouse hippocampus.** GAPDH/Aβ co-aggregate formation is shown. The hippocampus of a 3-month-old 3×Tg-AD mouse was subjected to insoluble fractionation and subsequently immunoprecipitated (IP) with an anti-Aβ antibody. This sample was analyzed by SDS-PAGE and Western blotting (*WB*) against GAPDH and Aβ. Values were calculated as the ratio of GAPDH (immunoprecipitated) band intensity (quantified in arbitrary units (*A.U.*)) relative to GAPDH (input) band intensity (*, $p < 0.05$, relative to the samples immunoprecipitated with control IgG, Student's *t* test).

Our data from 3×Tg-AD mice show co-localization of GAPDH aggregates with Aβ aggregates in extracellular deposits in the cortex. This co-localization was also observed in hippocampal CA3 pyramidal neurons and increased in an age-dependent manner (Fig. 7, *C* and *D*). The formation of Aβ/GAPDH co-aggregates was also quantitatively confirmed (Fig. 8). Aβ is produced by endoproteolysis of parental amyloid precursor protein and is secreted into the extracellular space (26). There is a substantial amount of evidence that Aβ can also accumulate intracellularly via several mechanisms, such as intracellular production and reuptake of extracellular Aβ (62). Secretion of GAPDH into the extracellular space has been previously reported (63). Therefore, extracellular and intracellular co-localization of GAPDH and Aβ aggregates both appear plausible.

Interestingly, 3×Tg-AD mice at 1 month of age showed evidence of GAPDH aggregation without Aβ aggregation in the hippocampal CA3 region (Fig. 7*C*). GAPDH aggregation, Aβ

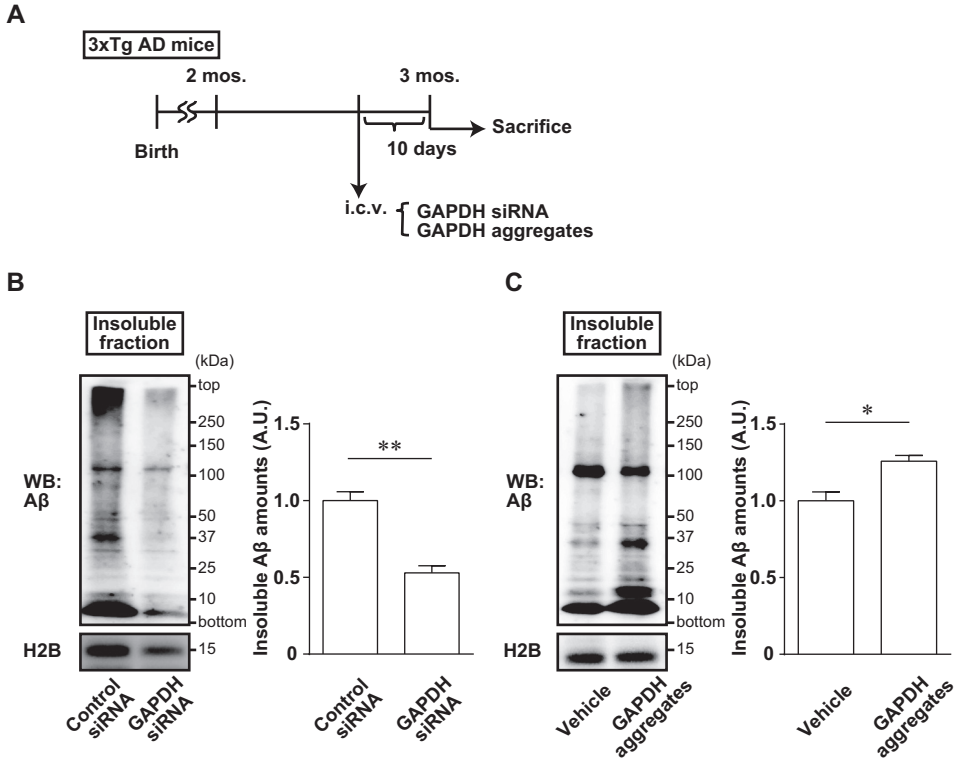

FIGURE 9. **GAPDH aggregates potentiate Aβ aggregate formation in the hippocampus of 3×Tg-AD mice.** *A,* schema indicating experiments following i.c.v. injection of GAPDH siRNA or GAPDH aggregates. 3×Tg-AD mice were i.c.v. injected with GAPDH siRNA or GAPDH aggregates. Ten days after injection (at 3 months of age), mice were sacrificed and subjected to insoluble fractionation followed by Western blotting. *B,* effect of GAPDH knockdown on Aβ aggregation in 3×Tg-AD mice was investigated by Western blotting (*WB*) against Aβ and H2B. H2B was used as internal standard protein present in the insoluble fraction (**, $p < 0.01$, relative to the treatment with control siRNA, Student's *t* test). *C,* effect of treatment with GAPDH aggregates on Aβ aggregation in 3×Tg-AD mice was investigated by Western blotting against Aβ and H2B (*, $p < 0.05$, relative to vehicle treatment, Student's *t* test). *A.U.*, arbitrary units.

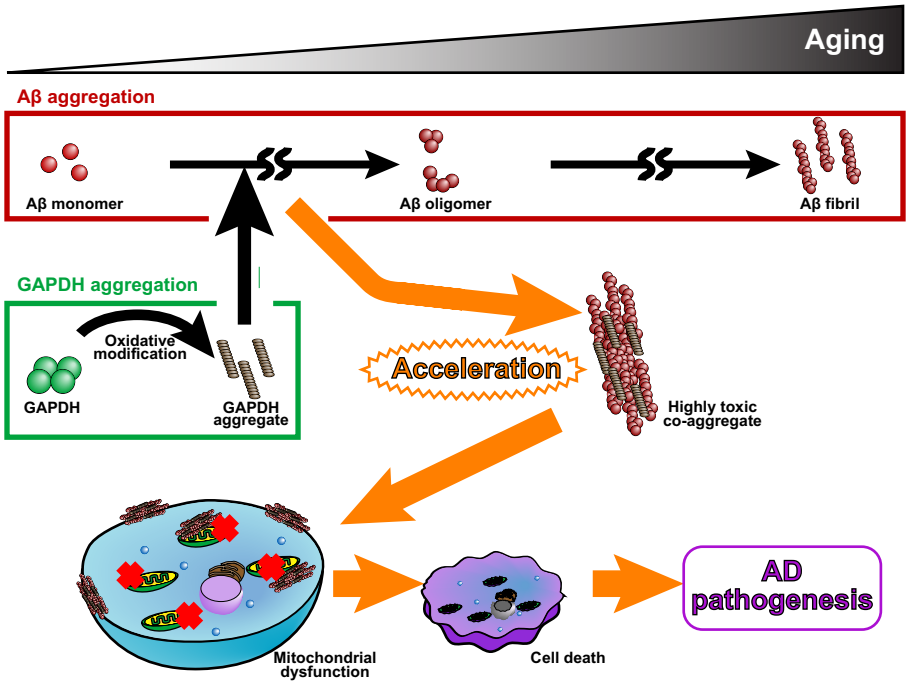

FIGURE 10. **Hypothetical model of the acceleration of Aβ amyloidogenesis by GAPDH aggregates in AD.** Oxidative stress-induced GAPDH aggregation occurs in the early phase of aging, interacting with soluble Aβ or early-stage Aβ oligomers. In AD, this interaction promotes an increase in the β-sheet content of Aβ, and initiates formation of toxic Aβ conformations. In the middle-to-late phase of aging, more toxic Aβ conformations, such as β-sheet-rich oligomers or fibrils (*i.e.* highly toxic co-aggregation between GAPDH and Aβ), are formed. The Aβ conformations generated by GAPDH aggregates eventually cause neuronal cell death via disruption of mitochondrial membrane potential.

aggregation, and co-localization of the two increased in an age-dependent manner (Fig. 7, *C* and *D*). These results imply that GAPDH aggregates are mainly involved in the initiation of Aβ aggregation. This hypothesis is supported by evidence that GAPDH easily aggregates as a consequence of exposure to oxidative stress (7, 11).

How do GAPDH aggregates occur in 3×Tg-AD brain? Considering that control mice showed almost the same patterns of GAPDH aggregates in an age-dependent manner as 3×Tg-AD mice (Fig. 7, *C* and *D*), the formation of GAPDH aggregates in the hippocampal CA3 region seems to be age-dependent. Indeed, redox proteomics analyses of rat brains revealed the presence of oxidatively modified GAPDH associated with changes in redox status during the aging process (64). Therefore, emergence of GAPDH aggregates in 3×Tg-AD mice might depend on normal brain aging rather than its triple mutant phenotype.

Taking into consideration the fact that several proteins known to co-localize with Aβ deposits, such as α-synuclein, prion protein, and cystatin C, regulate (either accelerate or inhibit) Aβ aggregation (65), it is possible that GAPDH also facilitates Aβ aggregation. Furthermore, from the results obtained from experiments using the i.c.v. injection of either GAPDH siRNA or GAPDH aggregates in 3×Tg-AD mice (Fig. 9), we suggest that GAPDH aggregates play a significant pathophysiological role in Aβ aggregation in AD pathogenesis.

In summary, this study demonstrates that GAPDH aggregates augment Aβ40 amyloidogenesis and promote Aβ40-induced cell death, accompanied by mitochondrial dysfunction *in vitro* and *in vivo* (Fig. 10). Moreover, co-localization of GAPDH/Aβ aggregates was observed in the cortices and hippocampi of 3×Tg-AD mice. These findings suggest that interaction between GAPDH aggregates and Aβ40 might be involved, at least in part, in the pathogenesis of AD.

Author Contributions—H. N., M. I., and T. T. designed the study; M. I., H. N., T. K., Y. S., S. H., A. Kaneshige, N. H., A. Kita, and R. Y. performed biochemical, cell-based, and animal tests (Figs. 1–9); T. K. and M. K. contributed to the Congo red analysis (Fig. 2); Y. S. and T. K. performed the AFM analysis (Fig. 2); S. K., H. N., and T. I. measured CD spectra (Fig. 2); M. I., T. K., Y-T. A., and M. K. contributed to the animal test analysis (Figs. 4–7); M. I., H. N., T. K., A. Kaneshige, and Y-T. A. analyzed data (Figs. 1–9); and H. N., M. I., T. I., and T. T. wrote the paper and graphical abstract (Fig. 10). All authors reviewed the results and approved the final version of the manuscript.

Acknowledgments—We thank Drs. Andreas Pluckthum and Peter Lindner (Zurich University) for providing W3CG.

References

1. Meyer-Siegler, K., Mauro, D. J., Seal, G., Wurzer, J., deRiel, J. K., and Sirover, M. A. (1991) A human nuclear uracil DNA glycosylase is the 37-kDa subunit of glyceraldehyde-3-phosphate dehydrogenase. *Proc. Natl. Acad. Sci. U.S.A.* **88,** 8460–8464
2. Zheng, L., Roeder, R. G., and Luo, Y. (2003) S phase activation of the histone H2B promoter by OCA-S, a coactivator complex that contains GAPDH as a key component. *Cell* **114,** 255–266
3. Tisdale, E. J. (2001) Glyceraldehyde-3-phosphate dehydrogenase is required for vesicular transport in the early secretory pathway. *J. Biol. Chem.* **276,** 2480–2486
4. Colell, A., Ricci, J.-E., Tait, S., Milasta, S., Maurer, U., Bouchier-Hayes, L., Fitzgerald, P., Guio-Carrion, A., Waterhouse, N. J., Li, C. W., Mari, B., Barbry, P., Newmeyer, D. D., Beere, H. M., and Green, D. R. (2007)

GAPDH and autophagy preserve survival after apoptotic cytochrome *c* release in the absence of caspase activation. *Cell* **129,** 983–997
5. Hara, M. R., Agrawal, N., Kim, S. F., Cascio, M. B., Fujimuro, M., Ozeki, Y., Takahashi, M., Cheah, J. H., Tankou, S. K., Hester, L. D., Ferris, C. D., Hayward, S. D., Snyder, S. H., and Sawa, A. (2005) *S*-Nitrosylated GAPDH initiates apoptotic cell death by nuclear translocation following Siah1 binding. *Nat. Cell Biol.* **7,** 665–674
6. Ishitani, R., Tanaka, M., Sunaga, K., Katsube, N., and Chuang, D.-M. (1998) Nuclear localization of overexpressed glyceraldehyde-3-phosphate dehydrogenase in cultured cerebellar neurons undergoing apoptosis. *Mol. Pharmacol.* **53,** 701–707
7. Nakajima, H., Amano, W., Fujita, A., Fukuhara, A., Azuma, Y.-T., Hata, F., Inui, T., and Takeuchi, T. (2007) The active site cysteine of the proapoptotic protein glyceraldehyde-3-phosphate dehydrogenase is essential in oxidative stress-induced aggregation and cell death. *J. Biol. Chem.* **282,** 26562–26574
8. Nakajima, H., Kubo, T., Ihara, H., Hikida, T., Danjo, T., Nakatsuji, M., Shahani, N., Itakura, M., Ono, Y., Azuma, Y. T., Inui, T., Kamiya, A., Sawa, A., and Takeuchi, T. (2015) Nuclear-translocated glyceraldehyde-3-phosphate dehydrogenase promotes poly(ADP-ribose) polymerase-1 activation during oxidative/nitrosative stress in stroke. *J. Biol. Chem.* **290,** 14493–14503
9. Sen, N., Hara, M. R., Kornberg, M. D., Cascio, M. B., Bae, B. I., Shahani, N., Thomas, B., Dawson, T. M., Dawson, V. L., Snyder, S. H., and Sawa, A. (2008) Nitric oxide-induced nuclear GAPDH activates p300/CBP and mediates apoptosis. *Nat. Cell Biol.* **10,** 866–873
10. Nakajima, H., Amano, W., Fukuhara, A., Kubo, T., Misaki, S., Azuma, Y.-T., Inui, T., and Takeuchi, T. (2009) An aggregate-prone mutant of human glyceraldehyde-3-phosphate dehydrogenase augments oxidative stress-induced cell death in SH-SY5Y cells. *Biochem. Biophys. Res. Commun.* **390,** 1066–1071
11. Nakajima, H., Amano, W., Kubo, T., Fukuhara, A., Ihara, H., Azuma, Y.-T., Tajima, H., Inui, T., Sawa, A., and Takeuchi, T. (2009) Glyceraldehyde-3-phosphate dehydrogenase aggregate formation participates in oxidative stress-induced cell death. *J. Biol. Chem.* **284,** 34331–34341
12. Forman, M. S., Trojanowski, J. Q., and Lee, V. M. (2004) Neurodegenerative diseases: a decade of discoveries paves the way for therapeutic breakthroughs. *Nat. Med.* **10,** 1055–1063
13. Ross, C. A., and Poirier, M. A. (2004) Protein aggregation and neurodegenerative disease. *Nat. Med.* **10,** S10–S17
14. Goto, A., Wang, Y.-L., Kabuta, T., Setsuie, R., Osaka, H., Sawa, A., Ishiura, S., and Wada, K. (2009) Proteomic and histochemical analysis of proteins involved in the dying-back-type of axonal degeneration in the gracile axonal dystrophy (gad) mouse. *Neurochem. Int.* **54,** 330–338
15. Pierce, A., Mirzaei, H., Muller, F., De Waal, E., Taylor, A. B., Leonard, S., Van Remmen, H., Regnier, F., Richardson, A., and Chaudhuri, A. (2008) GAPDH is conformationally and functionally altered in association with oxidative stress in mouse models of amyotrophic lateral sclerosis. *J. Mol. Biol.* **382,** 1195–1210
16. Tsuchiya, K., Tajima, H., Kuwae, T., Takeshima, T., Nakano, T., Tanaka, M., Sunaga, K., Fukuhara, Y., Nakashima, K., Ohama, E., Mochizuki, H., Mizuno, Y., Katsube, N., and Ishitani, R. (2005) Pro-apoptotic protein glyceraldehyde-3-phosphate dehydrogenase promotes the formation of Lewy body-like inclusions. *Eur. J. Neurosci.* **21,** 317–326
17. Wang, Q., Woltjer, R. L., Cimino, P. J., Pan, C., Montine, K. S., Zhang, J., and Montine, T. J. (2005) Proteomic analysis of neurofibrillary tangles in Alzheimer disease identifies GAPDH as a detergent-insoluble paired helical filament tau binding protein. *FASEB J.* **19,** 869–871
18. Cumming, R. C., and Schubert, D. (2005) Amyloid-β induces disulfide bonding and aggregation of GAPDH in Alzheimer's disease. *FASEB J.* **19,** 2060–2062
19. Ishitani, R., Tajima, H., Takata, H., Tsuchiya, K., Kuwae, T., Yamada, M., Takahashi, H., Tatton, N. A., and Katsube, N. (2003) Proapoptotic protein glyceraldehyde-3-phosphate dehydrogenase: a possible site of action of antiapoptotic drugs. *Prog. Neuropsychopharmacol. Biol. Psychiatry* **27,** 291–301
20. Li, Y., Nowotny, P., Holmans, P., Smemo, S., Kauwe, J. S., Hinrichs, A. L., Tacey, K., Doil, L., van Luchene, R., Garcia, V., Rowland, C., Schrodi, S., Leong, D., Gogic, G., Chan, J., et al. (2004) Association of late-onset Alzheimer's disease with genetic variation in multiple members of the GAPD gene family. *Proc. Natl. Acad. Sci. U.S.A.* **101,** 15688–15693
21. Lin, P. I., Martin, E. R., Bronson, P. G., Browning-Large, C., Small, G. W., Schmechel, D. E., Welsh-Bohmer, K. A., Haines, J. L., Gilbert, J. R., and Pericak-Vance, M. A. (2006) Exploring the association of glyceraldehyde-3-phosphate dehydrogenase gene and Alzheimer disease. *Neurology* **67,** 64–68
22. Tsuchiya, K., Tajima, H., Yamada, M., Takahashi, H., Kuwae, T., Sunaga, K., Katsube, N., and Ishitani, R. (2004) Disclosure of a pro-apoptotic glyceraldehyde-3-phosphate dehydrogenase promoter: anti-dementia drugs depress its activation in apoptosis. *Life Sci.* **74,** 3245–3258
23. Xu, G., Stevens, S. M., Jr., Moore, B. D., McClung, S., and Borchelt, D. R. (2013) Cytosolic proteins lose solubility as amyloid deposits in a transgenic mouse model of Alzheimer-type amyloidosis. *Hum. Mol. Genet.* **22,** 2765–2774
24. Butterfield, D. A., Swomley, A. M., and Sultana, R. (2013) Amyloid β-peptide (1–42)-induced oxidative stress in Alzheimer disease: importance in disease pathogenesis and progression. *Antioxid. Redox Signal.* **19,** 823–835
25. Oddo, S., Caccamo, A., Shepherd, J. D., Murphy, M. P., Golde, T. E., Kayed, R., Metherate, R., Mattson, M. P., Akbari, Y., and LaFerla, F. M. (2003) Triple-transgenic model of Alzheimer's disease with plaques and tangles: intracellular Aβ and synaptic dysfunction. *Neuron* **39,** 409–421
26. Scheuner, D., Eckman, C., Jensen, M., Song, X., Citron, M., Suzuki, N., Bird, T. D., Hardy, J., Hutton, M., Kukull, W., Larson, E., Levy-Lahad, E., Viitanen, M., Peskind, E., Poorkaj, P., *et al.* (1996) Secreted amyloid β-protein similar to that in the senile plaques of Alzheimer's disease is increased *in vivo* by the presenilin 1 and 2 and APP mutations linked to familial Alzheimer's disease. *Nat. Med.* **2,** 864–870
27. Small, D. H., Mok, S. S., and Bornstein, J. C. (2001) Alzheimer's disease and Aβ toxicity: from top to bottom. *Nat. Rev. Neurosci.* **2,** 595–598
28. Serpell, L. C. (2000) Alzheimer's amyloid fibrils: structure and assembly. *Biochim. Biophys. Acta* **1502,** 16–30
29. Lin, M. T., and Beal, M. F. (2006) Mitochondrial dysfunction and oxidative stress in neurodegenerative diseases. *Nature* **443,** 787–795
30. Butterfield, S. M., and Lashuel, H. A. (2010) Amyloidogenic protein–membrane interactions: mechanistic insight from model systems. *Angew. Chem. Int. Ed. Engl.* **49,** 5628–5654
31. Pagani, L., and Eckert, A. (2011) Amyloid-β interaction with mitochondria. *Int. J. Alzheimers Dis.* **2011,** 925050
32. Moreira, P. I., Carvalho, C., Zhu, X., Smith, M. A., and Perry, G. (2010) Mitochondrial dysfunction is a trigger of Alzheimer's disease pathophysiology. *Biochim. Biophys. Acta* **1802,** 2–10
33. Allen, M., Cox, C., Belbin, O., Ma, L., Bisceglio, G. D., Wilcox, S. L., Howell, C. C., Hunter, T. A., Culley, O., Walker, L. P., Carrasquillo, M. M., Dickson, D. W., Petersen, R. C., Graff-Radford, N. R., Younkin, S. G., and Ertekin-Taner, N. (2012) Association and heterogeneity at the GAPDH locus in Alzheimer's disease. *Neurobiol. Aging* **33,** 203.e225–233
34. Butterfield, D. A., Hardas, S. S., and Lange, M. L. (2010) Oxidatively modified glyceraldehyde-3-phosphate dehydrogenase (GAPDH) and Alzheimer's disease: many pathways to neurodegeneration. *J. Alzheimers Dis.* **20,** 369–393
35. Foley, A. M., Ammar, Z. M., Lee, R. H., and Mitchell, C. S. (2015) Systematic review of the relationship between amyloid-β levels and measures of transgenic mouse cognitive deficit in Alzheimer's disease. *J. Alzheimers Dis.* **44,** 787–795
36. Yamaji, R., Fujita, K., Takahashi, S., Yoneda, H., Nagao, K., Masuda, W., Naito, M., Tsuruo, T., Miyatake, K., Inui, H., and Nakano, Y. (2003) Hypoxia up-regulates glyceraldehyde-3-phosphate dehydrogenase in mouse brain capillary endothelial cells: involvement of Na^+/Ca^{2+} exchanger. *Biochim. Biophys. Acta* **1593,** 269–276
37. Ganter, C., and Plückthun, A. (1990) Glycine to alanine substitutions in helixes of glyceraldehyde-3-phosphate dehydrogenase: effects on stability. *Biochemistry* **29,** 9395–9402
38. Ono, K., Hirohata, M., and Yamada, M. (2005) Ferulic acid destabilizes preformed β-amyloid fibrils *in vitro*. *Biochem. Biophys. Res. Commun.* **336,** 444–449

39. Tanaka, M., Chien, P., Yonekura, K., and Weissman, J. S. (2005) Mechanism of cross-species prion transmission: an infectious conformation compatible with two highly divergent yeast prion proteins. *Cell* **121,** 49–62
40. Hong, H., and Liu, G. Q. (2004) Protection against hydrogen peroxide-induced cytotoxicity in PC12 cells by scutellarin. *Life Sci.* **74,** 2959–2973
41. Nilsson, M. R. (2004) Techniques to study amyloid fibril formation *in vitro*. *Methods* **34,** 151–160
42. Bucciantini, M., Giannoni, E., Chiti, F., Baroni, F., Formigli, L., Zurdo, J., Taddei, N., Ramponi, G., Dobson, C. M., and Stefani, M. (2002) Inherent toxicity of aggregates implies a common mechanism for protein misfolding diseases. *Nature* **416,** 507–511
43. Nagai, Y., Inui, T., Popiel, H. A., Fujikake, N., Hasegawa, K., Urade, Y., Goto, Y., Naiki, H., and Toda, T. (2007) A toxic monomeric conformer of the polyglutamine protein. *Nat. Struct. Mol. Biol.* **14,** 332–340
44. Gursky, O., and Aleshkov, S. (2000) Temperature-dependent β-sheet formation in β-amyloid Aβ(1–40) peptide in water: uncoupling β-structure folding from aggregation. *Biochim. Biophys. Acta* **1476,** 93–102
45. Mattson, M. P., Gleichmann, M., and Cheng, A. (2008) Mitochondria in neuroplasticity and neurological disorders. *Neuron* **60,** 748–766
46. Harkany, T., De Jong, G. I., Soós, K., Penke, B., Luiten, P. G., and Gulya, K. (1995) β-Amyloid(1–42) affects cholinergic but not parvalbumin-containing neurons in the septal complex of the rat. *Brain Res.* **698,** 270–274
47. Sloviter, R. S. (1989) Calcium-binding protein (calbindin-D28k) and parvalbumin immunocytochemistry: localization in the rat hippocampus with specific reference to the selective vulnerability of hippocampal neurons to seizure activity. *J. Comp. Neurol.* **280,** 183–196
48. Dong, Y. F., Kataoka, K., Tokutomi, Y., Nako, H., Nakamura, T., Toyama, K., Sueta, D., Koibuchi, N., Yamamoto, E., Ogawa, H., and Kim-Mitsuyama, S. (2011) Perindopril, a centrally active angiotensin-converting enzyme inhibitor, prevents cognitive impairment in mouse models of Alzheimer's disease. *FASEB J.* **25,** 2911–2920
49. Daugas, E., Susin, S. A., Zamzami, N., Ferri, K. F., Irinopoulou, T., Larochette, N., Prévost, M. C., Leber, B., Andrews, D., Penninger, J., and Kroemer, G. (2000) Mitochondrio-nuclear translocation of AIF in apoptosis and necrosis. *FASEB J.* **14,** 729–739
50. Wirths, O., and Bayer, T. A. (2012) Intraneuronal Aβ accumulation and neurodegeneration: lessons from transgenic models. *Life Sci.* **91,** 1148–1152
51. Hu, X., Crick, S. L., Bu, G., Frieden, C., Pappu, R. V., and Lee, J.-M. (2009) Amyloid seeds formed by cellular uptake, concentration, and aggregation of the amyloid-β peptide. *Proc. Natl. Acad. Sci. U.S.A.* **106,** 20324–20329
52. Seubert, P., Vigo-Pelfrey, C., Esch, F., Lee, M., Dovey, H., Davis, D., Sinha, S., Schlossmacher, M., Whaley, J., and Swindlehurst, C. (1992) Isolation and quantification of soluble Alzheimer's β-peptide from biological fluids. *Nature* **359,** 325–327
53. Harper, J. D., and Lansbury, P. T., Jr. (1997) Models of amyloid seeding in Alzheimer's disease and scrapie: mechanistic truths and physiological consequences of the time-dependent solubility of amyloid proteins. *Annu. Rev. Biochem.* **66,** 385–407
54. Jarrett, J. T., and Lansbury, P. T. (1993) Seeding "one-dimensional crystallization" of amyloid: a pathogenic mechanism in Alzheimer's disease and scrapie? *Cell* **73,** 1055–1058
55. Yanagisawa, K., Odaka, A., Suzuki, N., and Ihara, Y. (1995) GM1 ganglioside-bound amyloid β-protein (Aβ): a possible form of preamyloid in Alzheimer's disease. *Nat. Med.* **1,** 1062–1066
56. Grace, E. A., Rabiner, C. A., and Busciglio, J. (2002) Characterization of neuronal dystrophy induced by fibrillar amyloid β: implications for Alzheimer's disease. *Neuroscience* **114,** 265–273
57. Dahlgren, K. N., Manelli, A. M., Stine, W. B., Jr., Baker, L. K., Krafft, G. A., and LaDu, M. J. (2002) Oligomeric and fibrillar species of amyloid-β peptides differentially affect neuronal viability. *J. Biol. Chem.* **277,** 32046–32053
58. Tomiyama, T., Matsuyama, S., Iso, H., Umeda, T., Takuma, H., Ohnishi, K., Ishibashi, K., Teraoka, R., Sakama, N., Yamashita, T., Nishitsuji, K., Ito, K., Shimada, H., Lambert, M. P., Klein, W. L., and Mori, H. (2010) A mouse model of amyloid β oligomers: their contribution to synaptic alteration, abnormal tau phosphorylation, glial activation, and neuronal loss *in vivo*. *J. Neurosci.* **30,** 4845–4856
59. Bodles, A. M., Guthrie, D. J., Harriott, P., Campbell, P., and Irvine, G. B. (2000) Toxicity of non-Aβ component of Alzheimer's disease amyloid, and N-terminal fragments thereof, correlates to formation of β-sheet structure and fibrils. *Eur. J. Biochem.* **267,** 2186–2194
60. Simmons, L. K., May, P. C., Tomaselli, K. J., Rydel, R. E., Fuson, K. S., Brigham, E. F., Wright, S., Lieberburg, I., Becker, G. W., and Brems, D. N. (1994) Secondary structure of amyloid β peptide correlates with neurotoxic activity *in vitro*. *Mol. Pharmacol.* **45,** 373–379
61. Hayashi, H., Kimura, N., Yamaguchi, H., Hasegawa, K., Yokoseki, T., Shibata, M., Yamamoto, N., Michikawa, M., Yoshikawa, Y., Terao, K., Matsuzaki, K., Lemere, C. A., Selkoe, D. J., Naiki, H., and Yanagisawa, K. (2004) A seed for Alzheimer amyloid in the brain. *J. Neurosci.* **24,** 4894–4902
62. LaFerla, F. M., Green, K. N., and Oddo, S. (2007) Intracellular amyloid-β in Alzheimer's disease. *Nat. Rev. Neurosci.* **8,** 499–509
63. Yamaji, R., Chatani, E., Harada, N., Sugimoto, K., Inui, H., and Nakano, Y. (2005) Glyceraldehyde-3-phosphate dehydrogenase in the extracellular space inhibits cell spreading. *Biochim. Biophys. Acta* **1726,** 261–271
64. Perluigi, M., Di Domenico, F., Giorgi, A., Schininà, M. E., Coccia, R., Cini, C., Bellia, F., Cambria, M. T., Cornelius, C., Butterfield, D. A., and Calabrese, V. (2010) Redox proteomics in aging rat brain: involvement of mitochondrial reduced glutathione status and mitochondrial protein oxidation in the aging process. *J. Neurosci. Res.* **88,** 3498–3507
65. Eisenberg, D., and Jucker, M. (2012) The amyloid state of proteins in human diseases. *Cell* **148,** 1188–1203